



Review

High-Performance Room-Temperature Conductometric Gas Sensors: Materials and Strategies

Antonio Vázquez-López ^{1,2,†} , Javier Bartolomé ^{3,†}, Ana Cremades ¹ and David Maestre ^{1,*} 

¹ Department of Materials Physics, Universidad Complutense de Madrid, Plaza Ciencias 1, 28040 Madrid, Spain; antvaz01@ucm.es (A.V.-L.); cremades@fis.ucm.es (A.C.)

² IMDEA Materials Institute, C/Eric Kandel, 2, Getafe, 28906 Madrid, Spain

³ Department of Applied Physics, Universidad Autónoma de Madrid, C/Francisco Tomás y Valiente 7, 28049 Madrid, Spain; javier.bartolomev@uam.es

* Correspondence: dmaestre@ucm.es

† These authors contribute equally to this work.

Abstract: Chemiresistive sensors have gained increasing interest in recent years due to the necessity of low-cost, effective, high-performance gas sensors to detect volatile organic compounds (VOC) and other harmful pollutants. While most of the gas sensing technologies rely on the use of high operation temperatures, which increase usage cost and decrease efficiency due to high power consumption, a particular subset of gas sensors can operate at room temperature (RT). Current approaches are aimed at the development of high-sensitivity and multiple-selectivity room-temperature sensors, where substantial research efforts have been conducted. However, fewer studies presents the specific mechanism of action on why those particular materials can work at room temperature and how to both enhance and optimize their RT performance. Herein, we present strategies to achieve RT gas sensing for various materials, such as metals and metal oxides (MOs), as well as some of the most promising candidates, such as polymers and hybrid composites. Finally, the future promising outlook on this technology is discussed.

Keywords: room temperature; RT; gas sensing; chemiresistive; chemresistive; conductometric; conductive polymers; metal oxides; light activated; heterojunctions; morphology optimization; sensing principles



Citation: Vázquez-López, A.; Bartolomé, J.; Cremades, A.; Maestre, D. High-Performance Room-Temperature Conductometric Gas Sensors: Materials and Strategies. *Chemosensors* **2022**, *10*, 227. <https://doi.org/10.3390/chemosensors10060227>

Academic Editors: Nuno Santos and Joana Rodrigues

Received: 11 May 2022

Accepted: 14 June 2022

Published: 15 June 2022

Publisher's Note: MDPI stays neutral with regard to jurisdictional claims in published maps and institutional affiliations.



Copyright: © 2022 by the authors. Licensee MDPI, Basel, Switzerland. This article is an open access article distributed under the terms and conditions of the Creative Commons Attribution (CC BY) license (<https://creativecommons.org/licenses/by/4.0/>).

1. Introduction

Under the current global ecological crisis, there is an increasing need to take actions directed to detect, control, and reduce the emission of contaminants coming from a wide variety of sources and in diverse forms. Pollution monitoring is at the basis of any control action, and it is essential to minimize its effect on human health and the environment. Tackling this challenging objective requires the development of a battery of different sensors, each designed to work on a specific environment and target pollutant. In particular, air quality surveillance has become more and more demanding as more stringent limits have been imposed, not only for confined indoor areas, such as industrial or laboratory facilities, but also in ample outdoor spaces, such as urban environments or the countryside, where air pollution has been recognized as an important human health issue, at the same level as unhealthy diet or tobacco smoking [1,2]. Among the most common air pollutants, those posing higher risks for human health are SO₂, NO₂, O₃, CO, as well as volatile organic compounds (VOC), to name a few. Other compounds, such as NH₃, HCl, or H₂S, are also relevant in industrial or waste-treatment environments. Broadly speaking, the World Health Organization (WHO) recognizes two major gaps in the monitoring of air pollution levels, which limit the assessment of its impact on the environment and human health [1]. These gaps are the lack of sufficient monitoring posts in rural areas or outside major cities, and the extreme spatial variability occurring in the concentration of some pollutants (such

as NO₂), which render the normal sensor distribution within the cities insufficient to track their real levels. Thus, having a dense enough network of gas sensors capable of monitoring the concentration of these compounds in real time becomes essential to develop strategies for air pollution control, including human health risk prevention, as well as to improve the existing models for pollutant diffusion and propagation [3,4]. Implementing such a network will require the use of a large number of gas sensors, which, therefore, must be, at the same time, reliable and highly sensitive, while presenting low production costs and power consumption. Conductometric (also called chemresistive or resistive) gas sensors meet all these requirements, adding some more advantages, such as simplicity in fabrication, high robustness, and very low volume, making them an excellent choice for this mission [5–7]. With the advent and maturity of new thin film technologies and, later on, of nanoparticle films, significant improvements in their performance and capabilities have been achieved, resulting in their widespread use from industrial manufacturing to security or environmental monitoring [5,7], with a global market of USD 2330M in 2020 and an expected growth between 2019 and 2025 of 7.8%, according to the report of Grand View Research [8]. This has also translated into a constant increase in the number of published works related to this topic since the mid-2000s (Figure 1).

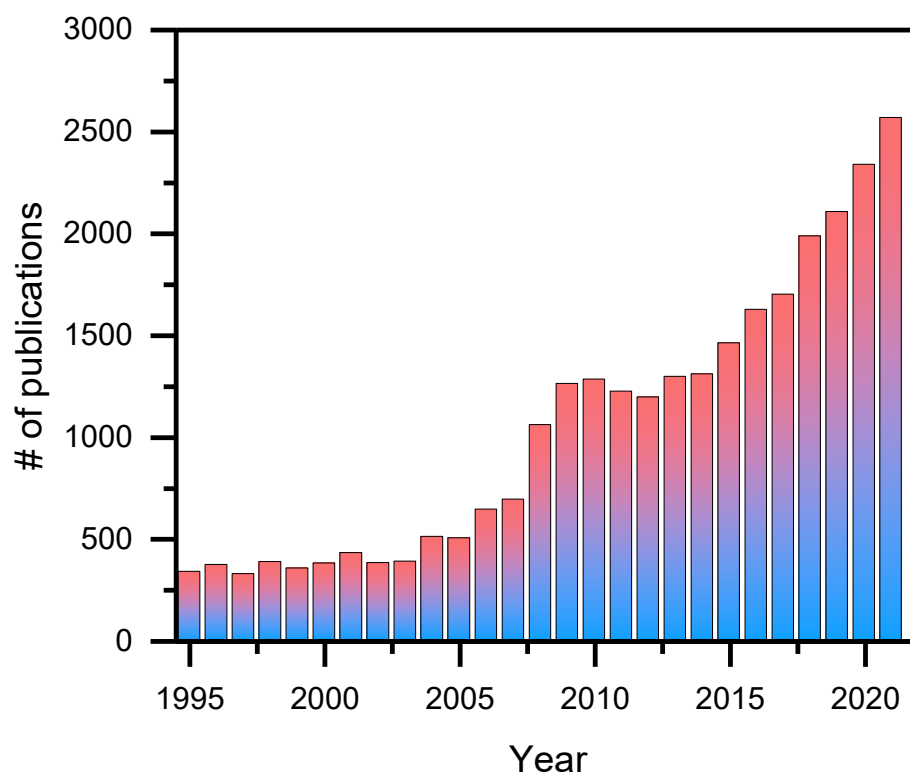


Figure 1. Number of publications in the area of gas sensors from 1995 to 2021 (data gathered from Scopus database).

The transducing mechanism of any conductometric gas sensor is based on the modulation of their electrical conductivity, regulated by changes in the composition of its surrounding atmosphere. Other relevant technologies in the field of gas sensing are classified by their transducing mechanism: optical sensors, chemical sensors, optochemical sensors, or electrochemical sensors [5,6,9]. Each of these technologies present intrinsic advantages in relation with conductometric sensors, but also specific drawbacks that limit their use in dense monitoring networks, such as high volumes or expensive manufacturing costs in the case of optical or optochemical sensors, lack of reusability in the case of chemical sensors, or stringent operation conditions and easy degradation in the case of electrochemical sensors [5]. A more comprehensive relation of the specific advantages and drawbacks

of these technologies can be found in Refs. [5,6,9]. In the particular case of conductometric gas sensors, their major disadvantages are their low specificity compared to some of their counterparts, their tendency to present temporal drifts, requiring periodic calibrations, and their high operation temperature, which imply larger power consumptions [5,10]. These drawbacks limit their practical use and overcoming them has become one of the major goals in the field of conductometric gas sensors.

The vast majority of conductometric gas sensors are based on semiconducting metal oxides (MOs) [6,7,11–13]. The reasons for this are their tunable transport properties and the high sensitivity of their surface electronic properties to changes in the composition of the surrounding atmosphere [13], caused by their large stoichiometry variability (i.e., presence of oxygen or cationic vacancies) [14], their relatively large catalytic activity, and, in some cases, the presence of different cationic oxidation states. Despite the great success of MOs as conductometric gas sensors, their employment as active (i.e., sensing) material is weighted down by their usual high operation temperature (>150 °C), which is used to both improve their sensitivity and response/recovery times, and to mitigate the interference caused by their high sensitivity to humidity [13]. High temperature operation imposes a significant energy toll, limiting the number of devices that can be installed as well as the number of viable locations. Besides, higher operation temperature can also induce poor stability. Thus, in order to improve the energy efficiency of conductometric gas sensors, it is essential to find new strategies to reduce their operation temperature down to room temperature (RT). The aim of this work is to summarize the most recent advances on room temperature conductometric gas sensing for environmental monitoring, including the use of new materials beyond conventional MOs and the development of novel strategies to achieve effective RT operation. While several reviews have been published on the topic of conductometric gas sensors [6,13,15,16], most of them mainly focused on recent advances and novel materials for RT operation; herein, we also focus on the most common strategies to obtain RT operation and the physical and chemical explanation of these phenomena. Thus, for some materials, such as MOs, strategies, such as the optimization of their dimension and morphology, could enhance its RT operation. The use of materials, such as polymers, and the formation of inorganic/organic composites is also here reviewed, as it becomes one of the main approaches to reach RT operation.

2. Sensing Principle and Mechanisms

The general operation principle of any conductometric gas sensor is based on the modulation of its majority carrier density through interaction with the analyte, and can be regarded as a charge injection/extraction process caused by the interaction between the analyte and the sensor surface, which, in turn, modifies the overall conductivity of the sensor. There are several different mechanisms that can lead to this charge exchange process, including direct charge transfer between the analyte and the sensor surface (Figure 2A) [17,18], the catalytic decomposition of the analyte and its chemical reaction with other adsorbed species (Figure 2B) [19,20], redox reactions between the analyte and the sensor (Figure 2C) [21,22], or the competition for adsorption sites with other adsorbed species (Figure 2D) [23], among others. This charge exchange process may tune the overall conductivity of the sensor directly by varying the net concentration of available free carriers [13,17,18] (n for electrons, p for holes), according to:

$$\sigma = e(\mu_n n + \mu_p p) \quad (1)$$

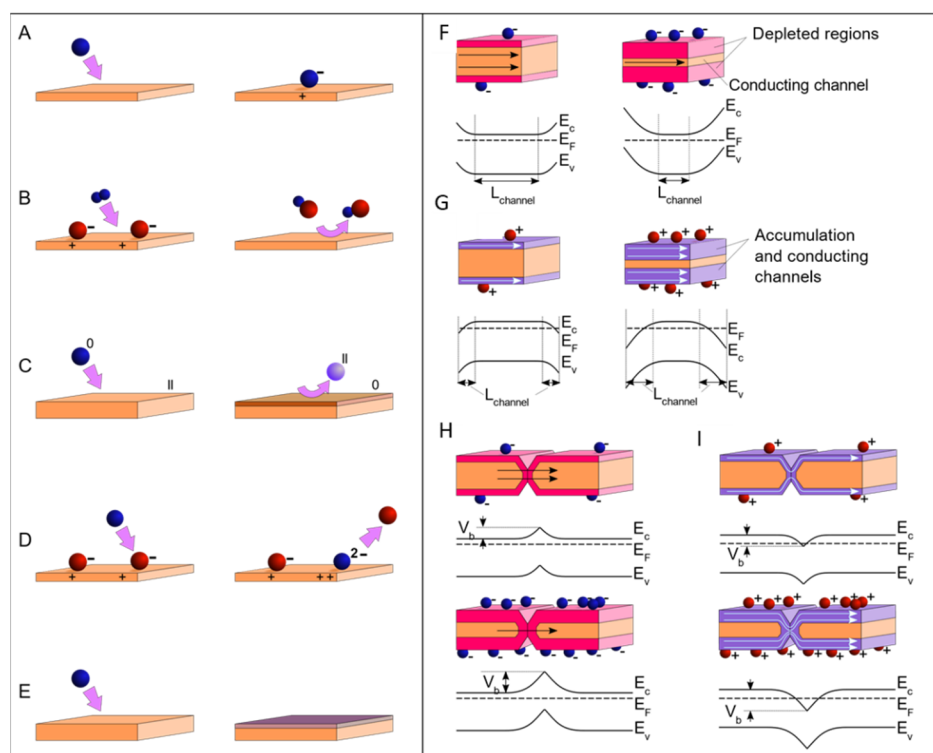


Figure 2. Left: Different analyte–sensor interaction processes: (A) direct charge transfer through ionosorption, (B) catalytic decomposition of the analyte and chemical reaction with other adsorbed species, (C) redox reactions between the analyte and the sensor surface, (D) competition for the same adsorption sites with other adsorbed species, and (E) (reversible) chemical reaction. Right: effect of space charge regions on the sensor conductivity (for an n-type semiconductor): (F,G) formation of conduction channels and (H,I) formation of potential junction barriers between two adjacent grains.

Here, μ is the mobility of the corresponding free carrier type, and e the elemental charge. This mechanism and its implication on the overall sensor performance were explored in detail by P. Moseley in Ref [13], who showed that in this case scenario, the response is strongly influenced by the material's bulk donor density, N_D , with a linear dependence on the concentration of analyte for pure n- (high N_D) or p-type (low N_D) materials and a mixed behavior for intermediate N_D values (Figure 3). Most commonly, however, the conductance is affected by the formation of space charge regions in the form of depletion or accumulation layers due to surface band bending effects [24–26]. The impact of these space charge regions depends strongly on the microstructure of the sensor. For polycrystalline materials with grain sizes comparable to their Debye lengths, the appearance of depletion regions induces the formation of conduction channels (Figure 2F, the width of which is regulated by these charge injection/extraction processes [26]). Similarly, accumulation layers would act as preferential conduction paths (Figure 2G) with variable width [27]. For larger crystalline sizes, and in the presence of depletion regions, conduction becomes limited by the appearance of voltage barriers at the grain boundaries (Figure 2H). In this case, the injection/extraction of carriers modifies the height of the barrier, which determines the overall conduction through the grain boundary [28]. Conversely, the formation of accumulation layers at grain boundaries has the effect of providing low-resistivity conduction paths, similar to the small-crystalline-size scenario. This difference in the control of the conductivity for the same microstructure translates into different sensitivities for the same band bending, V_b (in absolute value), caused by the adsorption of the analyte, depending on whether it causes the depletion or the accumulation of free carriers, according to [27]:

$$S_a = \sqrt{S_d} \quad (2)$$

where S_a is the sensitivity for the case in which accumulation layers are formed, and S_d is the sensitivity for the formation of depletion layers. Thus, control on the carrier density and microstructure of the active material is crucial to optimize the sensor response.

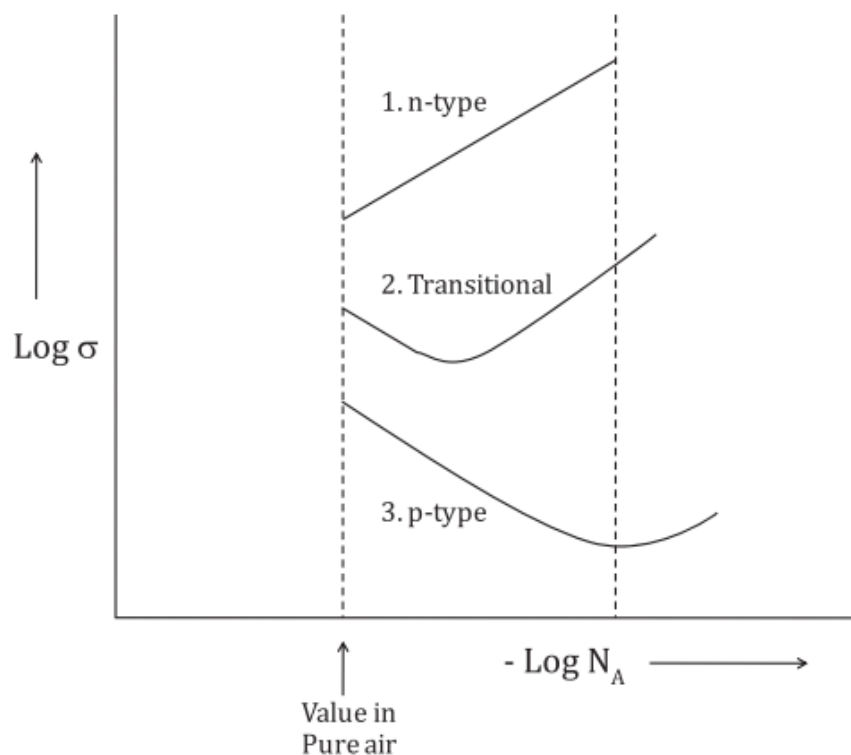


Figure 3. Conductivity dependence on the concentration of analyte (represented by the surface acceptor state density N_A per unit volume) for three materials with different bulk donor density N_D . Reprinted with permission from Ref. [13]. Copyright 2017, IOP Publishing.

A somewhat different process involves the formation of new chemical species by the reaction of the analyte with the sensor surface (Figure 2E). The new chemical species usually have different conductivity characteristics, which reflect on the overall conductivity of the sensor. This is the case, for instance, with highly active redox reactions in which the whole sensor surface changes its oxidation state, leading to the formation of a highly conducting metallic surface [29], but also has been observed in certain sulfuration reactions, such as those produced during H_2S detection by NiO sensors, in which the reversible NiS phase presents higher conductivities than its oxide counterpart [30]. It should be pointed out that other MOs have also shown great results detecting H_2S , such as CuO [31]. However, this mechanism is not very common, as chemical reactions must be fully reversible at operation conditions and recovery should proceed at a fast enough pace in order to ensure the proper functioning of the sensor.

Thus, each specific sensing mechanism results from the combination of a particular analyte–sensor interaction and its effect on the conductivity of the sensor. Usually, there is more than one sensing mechanism taking place at the same time during the conductometric response of any device [18,32]. For instance, Bartolomé et al. [18] showed the simultaneous operation of two different competing mechanisms during room temperature sensing of ethanol with p-type NiO, consisting on the catalytic decomposition of adsorbed ethanol on the NiO surface, and the direct charge transfer between both compounds, which lead to different responses, depending on the operation conditions. Which process or processes will eventually dominate the response would depend on the specific physical and chemical properties of the sample, as well as operation conditions (i.e., temperature, atmosphere, etc.).

In the case of MO-based sensors, the majority of these sensing mechanisms have been wrapped up in the so-called ionosorption model. According to this model, the overall charge exchange between the analyte and the sensor surface is governed by ionized adsorbed species. These species may be the analyte itself, but most commonly, the whole process is mediated by adsorbed oxygen ions, in the form of O_2^- , O^- , and O_2^{2-} , depending on the operation temperature [6], although at RT, the most relevant species is O_2^- . Oxygen adsorbs on the surface of any MO sensor, trapping an electron from it and, depending on the operation temperature, further decomposing into O^\bullet free radicals and/or trapping an additional electron. This creates an electron depletion layer on n-type MOs or a hole accumulation layer on p-type MOs, strongly impacting the conductivity of the sensor, through any part of the process described before. Reducing analytes usually react chemically with these ionosorbed oxygen species, which are then released in the form of reaction products, giving back the trapped electrons, while oxidizing analytes interact directly with the surface, trapping an electron from the sensor and, thus, becoming ionized [15,33]. A comprehensive mathematical description of these oxygen ionosorption processes, regarding equilibrium carrier concentration and sensor conductivity dependence on analyte concentration, was given by Barsan and Weimar in Ref [34] for the particular case of SnO_2 , which may be extrapolated for other materials as well. The ionosorption (sometimes called oxygen ionosorption) model has been used to successfully describe a wide number of sensor–analyte systems [13,27]; however, this has led to the unfortunate generalization of the terms “n-/p-type sensor” and “oxidizing/reducing analyte” in relation only to the observed response, without any further consideration of the actual physicochemical mechanisms taking place. This oversimplification of the overall sensing process may induce some misconceptions regarding the expected behavior and performance of the sensors towards specific analytes, sometimes leading to unexpected and even contradictory results. However, these results are entirely the consequence of the coexistence of several different sensing mechanisms that, once they are properly understood, can be exploited to develop a myriad of different MO gas sensors [17,18,23,30].

It is noteworthy that while the majority of the sensors can be described in the frame of the aforementioned mechanisms, some particular systems have specific sensing mechanisms that are not included in this overview. This is the case of novel organic sensors, which are discussed in Section 4, humidity sensors based on thick or ceramic films that governed the Grotthuss mechanism of proton hopping [35], or 2D material (2DM) sensors (such as graphene, s transition metal dichalcogenides (TMDs), metal dichalcogenides (MD), graphene oxide (GO), or MXenes), also described in Section 4, which may involve more complex behaviors by virtue of their peculiar physical properties.

3. Characterization Techniques for Studying Conductometric Gas Sensors

Due to the intrinsic surface nature of the analyte–sensor interaction, the study of any conductometric gas-sensing mechanism normally requires the employment of surface and/or chemically sensitive characterization techniques. Usually, the basic characterization of the samples is performed *ex situ*, recording the electrical response to the analyte separately from the rest of the characterization techniques. Despite this procedure being able to provide plenty of useful information, it hinders the proper identification of the relevant sensing mechanisms involved in the response due to the lack of correlation between the conductivity of the samples immersed in different atmospheres and the rest of their physical properties. Nonetheless, in recent years, this tendency has been progressively reversing with the establishment of new *in-situ/in-operando* measurements, particularly for MOs but also for organic and 2DM-based sensors, in which physical changes in both the sample (sensor) and the analyte are monitored during the sensing process, employing chemically sensitive techniques, such as Fourier transform infrared (FTIR) spectroscopy, diffuse reflectance infrared Fourier transform spectroscopy (DRIFTS), Raman spectroscopy, or X-ray photoelectron spectroscopy (XPS) in near ambient pressure (NAP) conditions [21,32,36–39]. DRIFT/FTIR and Raman spectroscopies may provide relevant information on the adsorp-

tion processes and chemical decomposition of the analyte on the surface of the sensor. Besides, 2DMs are very prone to be doped by adsorbed gases [40,41], so *in-operando* Raman spectroscopy as well as photoluminescence (PL) spectroscopy are excellent probes to follow the processes occurring during the whole gas-sensing cycle, as both techniques may be used to characterize their doping and strain state, particularly for graphene [42] and transition metal dichalcogenides (TDM) [43–45]. A review on the use of Raman spectroscopy for in-situ and *in-operando* studies of different gas sensors can be found in Ref. [46]. Similarly, XPS is a very powerful characterization tool, as it provides information on the surface chemistry of the sample and its electronic surface states, which strongly determine the kind of interaction that can take place between the sample and the analyte. However, contrary to (DR)FTIR/Raman spectroscopy, XPS requires ultra-high vacuum (UHV) conditions, which hinder the study of the sensing processes at normal operation conditions. Fortunately, the recent development of NAP-XPS has helped to bridge the gap between its normal ultra-high vacuum operation and ambient pressure operation of gas sensors, allowing the observation of analyte–sensor interactions in more realistic conditions, close to their normal operation in ambient conditions [36,37,47]. One major drawback of XPS is the need to use high-intensity, high-energy X-ray beams, which tend to degrade sensitive samples, such as organic-based sensors, limiting its applicability on these systems. In these cases, the use of in-situ (DR)FTIR/Raman spectroscopy becomes essential to understand the processes involved in the sensing response. The combination of several of these *in-operando* tools for the study of specific analyte–sensor systems has shown great potential in understanding the dynamic evolution of complex systems during the sensing process. For instance, Sänze et al. [21] employed a combination of *in-operando* FTIR and Raman spectroscopy measurements to unravel the chemical surface modifications of the sensor and the formation of different byproducts during ethanol, ethene, and acetaldehyde gas sensing with In_2O_3 thin films, depending on the sensing temperature and environmental oxygen partial pressure (Figure 4).

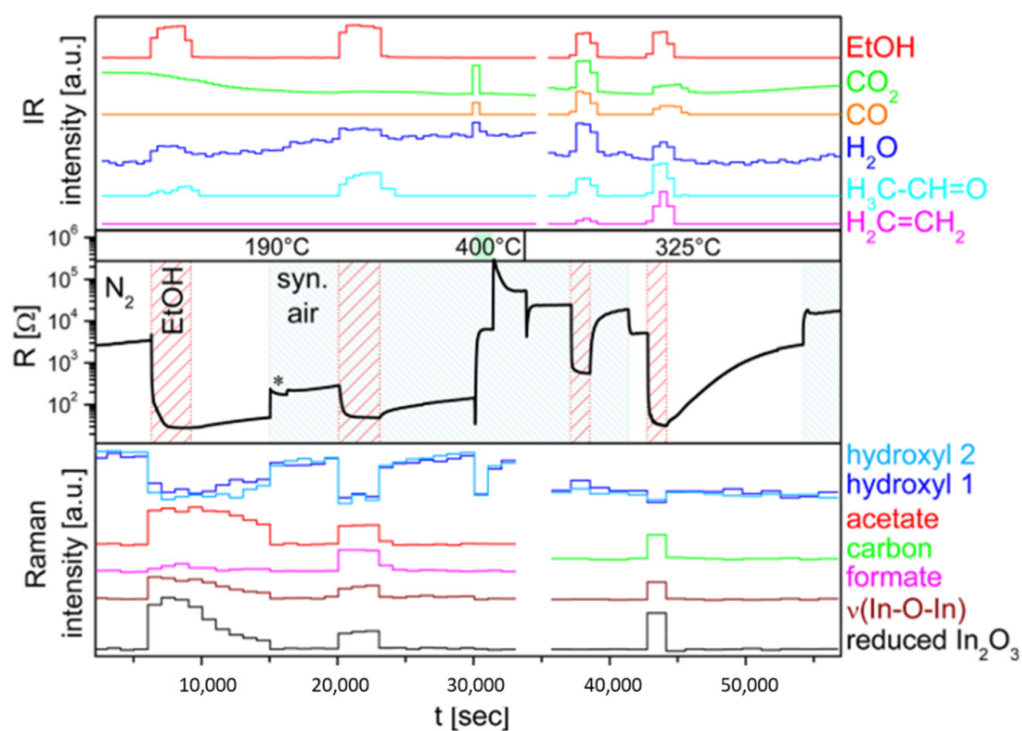


Figure 4. Correlative *in-operando* FTIR and Raman spectroscopy signals with sample resistance during ethanol exposure of indium oxide sensors. Adapted with permission from [21]. Copyright 2014, American Chemical Society.

4. Strategies for RT Operation

Room temperature operation is usually limited by the kind of sensing mechanism involved in the response and the sensitivity of the sample towards the presence of moisture. The dominant sensing mechanism determines both the sensitivity, S , of the sensor and its kinetics, i.e., the response and recovery times, τ_{res} and τ_{rec} . Sensor sensitivity is usually defined as either the ratio or the relative resistance difference between the resistance upon analyte exposure, R_g , and the base resistance R_0 :

$$S = \frac{R_g}{R_0} (\%), \quad S = \frac{R_g - R_0}{R_0} = \frac{\Delta R}{R_0} (\%) \quad (3)$$

When $R_g < R_0$, usually, the first definition is rewritten as the ratio between R_0 and R_g , in order to allow proper comparison between different response types, sometimes making unclear the actual direction of the resistance change, unless explicitly stated. Conversely, the second definition allows a direct comparison between positive and negative sensitivities without any expression reorganization, facilitating the discussion and also providing a more direct way to compare with the background noise in order to set the low detection limit of the sensor. Response and recovery times are usually defined as the time required to reach 90% of the final resistance value after either exposing the sensor to a stable concentration of the analyte or after completely withdrawing the analyte. According to this definition, it is necessary to let the signal stabilize after each change in analyte concentration in order to properly measure the value of τ_{res} and τ_{rec} . However, in many cases, large values of τ_{res} and τ_{rec} yield unsaturated response curves, which, in turn, lead to an underestimation of their value, hindering the assessment of the sensor performance. In these cases, extending the measuring time until the curves are fully saturated may not be an option, particularly in the presence of strong temporal drifts. A way to avoid this is to employ an alternative definition, assuming an exponential behavior and fitting the curves to a phenomenological expression [18]:

$$R = R_i + \Delta R \left(1 - e^{-t/\tau}\right) \quad (4)$$

where τ is either τ_{res} or τ_{rec} , R_i is, respectively, R_0 or R_g and ΔR is $R_0 \pm R_g$. This expression allows a direct estimation of the response and recovery times, even if the curves are not fully saturated, although it gives somewhat lower τ values, compared to the 90% definition.

Low-temperature operation, down to RT, tends to reduce the speed at which reactions take place at the surface of the sensors, negatively impacting both the sensitivity and the response/recovery time of the devices. Moreover, lower response and drifts in the sensing performance can also occur at room temperature. However, as explained before, some sensing mechanisms do not rely on chemical reactions at all, such as the case of direct charge transfer. In those cases, reducing the temperature might actually be beneficial [18]. In other cases, the sensitivity of the sensors is so high that room temperature operation is perfectly feasible. Sometimes, the adsorption/desorption speed may become the actual bottleneck for the overall sensor performance, and, hence, a different (more efficient) source of energy, such as ultraviolet (UV) illumination, may be employed in order to enhance these processes. Reducing the impact of humidity interference without heating the sensor usually requires the selection of humidity-impervious materials. Thus, several different strategies have been explored so far in order to achieve room temperature operation with conductometric gas sensors, although very often, two or more of these strategies are combined in order to obtain the best possible performance. Some of the strategies and the previously described parameters alongside with recent results are shown in Table 1.

Table 1. Summary of different reported strategies to achieve room temperature response for conductometric gas sensors.

Strategy	Type	Material	Structure	Gas	Concentration (ppm)	Sensitivity Equation	S	τ_{res}/τ_{rec} (s)	Ref.
Light activated		In ₂ O ₃	NPs film	O ₃	10	$S = \frac{R_{Ozone}}{R_{UV}}$	10 ⁵	>1/30	[24]
		TiO ₂	Fractal carbon + TiO ₂	Acetone	12.5	$S = \frac{R_0}{R_g}$	100	12/174	[48]
		ZnO		Acetone	0.1–1000	-	1–400	-	[49]
Specific sensing pathways		NiO	Ceramic	Ethanol	200–16,000	$S = \frac{\Delta R}{R_0}$	2	30.6/86.8	[18]
		In ₂ O ₃	NWs	H ₂ S	20	$S = \frac{R_0}{R_g}$	141.1	-	[50]
		In ₂ O ₃	NTs	H ₂ S	20	$S = \frac{R_0}{R_g}$	166.6	-	[50]
Morphology optimization	0D	PbS	QDs	NO ₂	30	$S = \frac{R_N}{R_g}$	11.8	13 s/14 min	[51]
	1D	Ag	NW	NH ₃	1–2	-	5	-	[52]
	1D	In ₂ O ₃	NW	NO ₂	0.02	-	25	-	[52]
	2D	SnS ₂	2D layers	NO ₂	8	$S = \frac{R_g}{R_0}$	10.8	164/236	[53]
Heterojunctions	2D/0D	rGO/CD	-	NO ₂			0.010–25	100/150	[54]
	2D/0D	SnS ₂ /SnO ₂	-	NH ₃			100–500	200/300	[54]
	2D/3D	rGO/n-Si	-	NO ₂			250–1000	100/200	[54]
	2D/3D	In ₂ O ₃ /SnO ₂	Nanorods	NO _x	0.1–100	$S = \frac{\Delta R}{R_g}$	0.1–9	4.67–8.98	[55]
Conductive polymer		PANI	-	NH ₃	50	$S = \frac{R_0}{R_g}$	2.6	290/-	[56]
		PEDOT:PSS/EG	Thin film	ethanol	200	$S = \frac{\Delta R}{R_0}$	0.2	-	[57, 58]
		PPy	Thin film	NH ₃	4–80	$S = \frac{R_g}{R_0}$	1.12	20 s/15 min	[59]
		PTh	Thin film	NO ₂	10–100	$S = \frac{R_g}{R_0}$	1.33	220/1603	[59]
Hybrid composite		PEDOT:PSS/AuNps		CH ₄	0.02–1		8.6	22/43	[60]
		PANI/CeO ₂		NH ₃	50	$S = \frac{R_0}{R_g}$	6.5	57.6/-	[56]
		PEDOT:PSS/EG/SnO		Ethanol	200	$S = \frac{\Delta R}{R_0}$	2.6	-	[57, 58]
		PEDOT:PSS/EG/SnO ₂		Ethanol	200	$S = \frac{\Delta R}{R_0}$	0.36	-	[58]
	PEDOT:PSS/EG/TiO ₂		Ethanol	200	$S = \frac{\Delta R}{R_0}$	0.9	-	[57]	

4.1. Light-Activated RT Operation

One of the most successful strategies directed to obtain RT gas sensors consists of the employment of light, typically in the range of UV to visible light, as an energy source to enhance some of the processes taking place during the sensing response [61,62]. There are currently several reviews available covering this particular topic from different perspectives [63–67], so here, we will try to summarize some of the most important aspects of this strategy. There are several ways by which UV and visible light can enhance the response of the sensors, but usually, they are all based on the generation of photocarriers that interact with the adsorbed analyte (Figure 5a–c). Depending on the role played by these photocarriers, two photoactivated enhancement mechanisms can be distinguished:

1. Analyte adsorption/desorption enhancement: this approach is used on highly sensitive sensors, which show good response times at RT but slow recoveries due to the slow desorption rate of the analyte. Photogenerated carriers may rapidly recombine with any adsorbed ionic species, either ionosorbed oxygen/analyte molecules or any ionized product formed during the decomposition of the analyte, causing them to desorb as neutral species and speeding up the recovery process. A theoretical model of the kinetics of the photo-enhanced desorption of oxygen on MOs was developed by Melnick [68] with ZnO as a case study. An example of such photoactivated RT gas sensing was demonstrated for In₂O₃ thin films with UV back-illumination for ozone detection (Figure 5d) [28]. By periodically switching on and off the UV light, the authors managed to modulate the desorption speed of the decomposed O₃ molecules. The measured resistance is then dependent on the equilibrium between the O₃ adsorption rate, which depends on the concentration of O₃ molecules, and the desorption rate, which depends on UV light illumination, i.e., on the ON/OFF state (Figure 5e). The obtained response, measured as the resistance ratio between the OFF (R_{O_3}) and the ON (R_{UV}) states for a given O₃ concentration, was found to vary linearly with O₃ concentration (Figure 5f).

2. Analyte reaction enhancement: this approach can be employed to enhance the response in gas sensors based on the catalytic decomposition of the analyte [67,69]. Many sensing mechanisms are based on the catalytic decomposition of the analyte on the sensor surface; the obtained subproducts may then either react with ionosorbed oxygen species, releasing trapped electrons, or trap free carriers themselves. These processes usually require high temperatures as a source of energy to proceed at reasonable speeds. Photocatalytic materials use photon energy instead to speed up the chemical decomposition of the analyte and promote their sensitivity at RT. In this case, photogenerated carriers interact with the analyte, breaking chemical bonds and promoting either their oxidation with ionosorbed oxygen species or their chemical reaction with other adsorbed species, such as H₂O or other decomposed products [70]. Many MOs are known to have photocatalytic properties, such as TiO₂ [48], SnO₂ [20], or ZnO [49], but also organic polymers [71] or 2D materials [72,73].

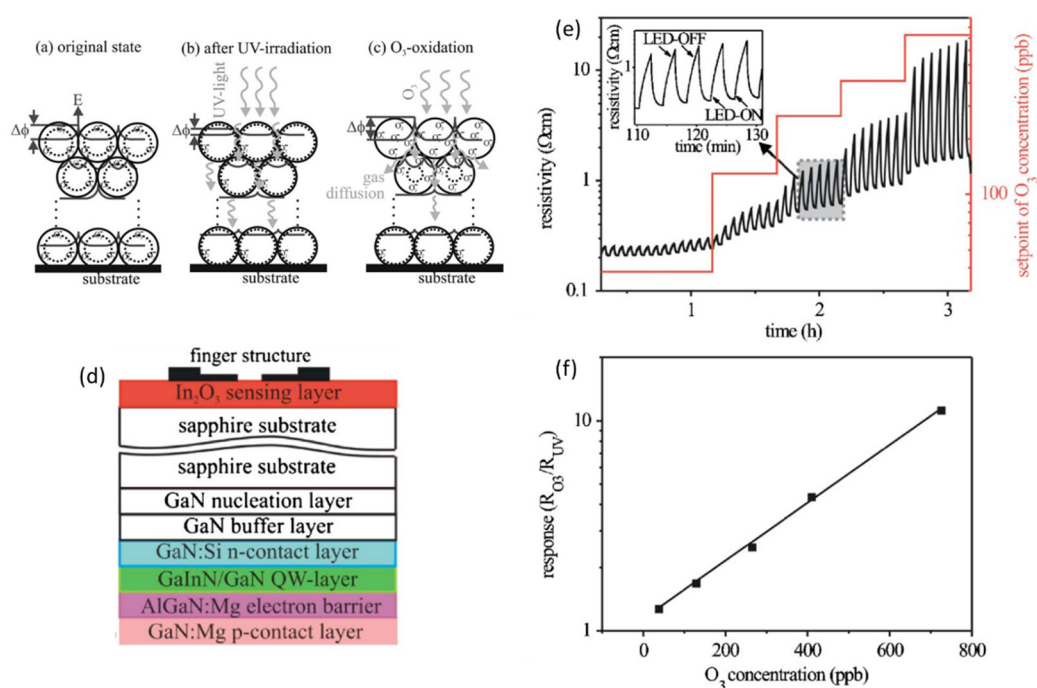


Figure 5. (a–c) Schematic of the steps followed during photoactivated sensing: the initially adsorbed oxygen species are forced to desorb from the sensor surface by UV illumination, releasing their trapped electrons into the n-type sensor (In₂O₃) and, thus, reducing the energy barrier between grains switching into a low-resistivity state. Exposure to an oxidizing analyte (O₃) recovers the initial high-resistance state by trapping, again, surface free electrons and increasing the energy barrier between grains. Reproduced with permission from [24]. Copyright 2007, American Institute of Physics. (d) Schematic of a photoactivated In₂O₃ sensor with integrated UV LED emitter (e,f) response signal and sensitivity of a photoactivated In₂O₃ sensor for ozone detection with pulsed UV operation. Reproduced with permission from [28]. Copyright 2007, American Institute of Physics.

Since sensor photoactivation requires the generation of photocarriers, the energy of the photons must be larger than the energy bandgap of the active material in order to promote electrons to form the valence band (VB) to the conduction band (CB), in the case of inorganic semiconducting sensors, or from the highest occupied molecular orbital (HOMO) to the lowest unoccupied molecular orbital (LUMO) in the case of organic sensors. Since many MOs have energy bandgaps well above 3 eV, within the UV region, the kind of illumination sources that can be used becomes very limited, not to mention their associated health risks. To overcome this problem, some strategies have been used, such as the employment of organic dyes [74] and quantum dot (QD) sensitizers [75], noble metal decoration for localized surface plasmon resonance (LSPR) light absorption

enhancement [76], or employing narrow bandgap MOs as sensitizer or directly as the active material [77].

While this method shows good results, it still requires an additional energy source to power the light emitter, which must be integrated in the sensor, increasing its complexity, and humidity interference is not always avoided, even at high UV irradiation intensities [63].

4.2. Specific Sensing Pathways

Other approaches make use of specific sensing mechanisms with enhanced RT responses, such as direct charge transfer between the analyte and the active material or particular chemical reactions that are favored at low temperature [18,50]. For instance, Bartolomé et al. showed that an enhanced ethanol sensing performance could be achieved at RT on NiO sensors, provided that the ethanol decomposition sensing path is blocked and only direct charge transfer is allowed between adsorbed ethanol molecules and the NiO surface [18]. Weakly physisorbed ethanol acts as an efficient electron trap by virtue of its strongly electronegative OH group, increasing the conductivity of p-type NiO. Due to its weak bonding to the surface, physisorbed ethanol can efficiently desorb after it has been removed from the surrounding atmosphere, yielding to short response and recovery times (Figure 6a). Conversely, when ethanol undergoes a dissociative chemisorption, the obtained subproducts can react with ionosorbed oxygen species, releasing their trapped electrons and producing an opposite behavior, which diminishes the overall sensitivity and increases the recovery time of the sensor (Figure 6b). This mechanism is the dominant one at high temperature, but at room temperature, it can be hampered by carefully selecting the microstructure and crystalline orientation of the sensing layer. A different route is exploited by Xu et al. on electrospun In_2O_3 nanowire and nanotube gas sensors for H_2S detection [50]. In this case, In_2O_3 undergoes a sulfuration reaction after being exposed to H_2S , reversibly transforming between In_2O_3 and In_2S_3 , following the reactions of Equations (5) and (6):

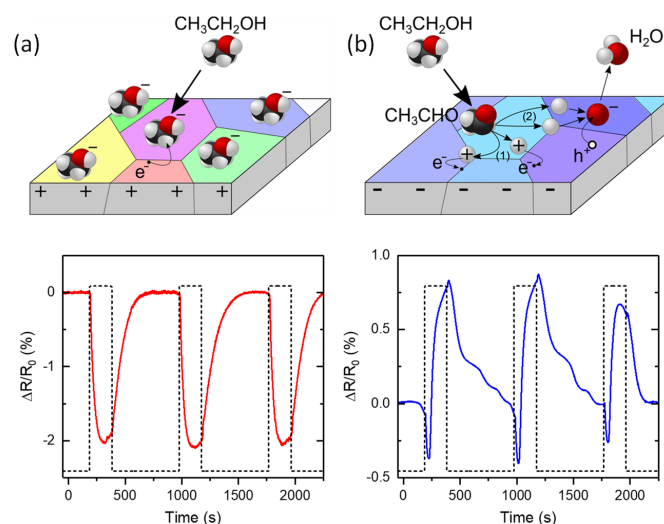
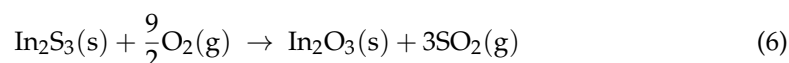
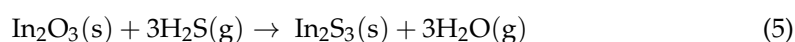


Figure 6. Oposing sensing mechanisms of NiO towards ethanol analyte at room temperature. (a) Direct charge transfer induces a resistance decrease in the sample with fast recoveries after removing the ethanol from the atmosphere. (b) Conventional catalytic decomposition of ethanol leads to the usual resistance increase with an associated much slower response and recovery time. Adapted with permission from [18]. Copyright by Elsevier (2022) under CC BY-NC-ND license.

These reactions are spontaneous at room temperature, with a negative Gibbs free energy difference, ΔG , which increases with temperature. As the temperature increases, ΔG , also increases, approaching to 0 and, thus, making the transformation less and less favorable. Thus, at room temperature, the sulfuration reaction dominates the response, with high sensitivities and low response/recovery times, while at high temperatures, the reduced speed of sulfuration reaction allows H_2S to also react directly with ionosorbed oxygen species through a more conventional, but also less-sensitive sensing mechanism, thus, having a combination of both mechanisms in the overall response.

One of the major disadvantages of these strategies is that they are very sensor-analyte specific, and their systematization requires a profound knowledge of the existing sensing mechanisms, which is still lacking for most of the materials systems, although some progress has been made in this direction over the last few years.

4.3. Morphology Optimization (0D, 1D, 2D)

Another way to enhance the response of conductometric gas sensors at RT is the use of optimized sensor morphologies. The central idea of this approach is that, on one hand, the higher the surface-to-volume ratio of the active layer, the higher the sensitivity and the better the response/recovery time will be for any given sensing mechanism; on the other hand, reducing the size of the active material close to its Debye length allows the formation of conduction channels that can be completely depleted or even inverted (in terms of majority carrier type) upon analyte adsorption [26,64]. This strategy has led to the development, over the last decade, of a vast amount of 0D and 1D nanostructured materials for gas sensing, including the fabrication of nanoparticle thin films, presenting a large variety of morphologies, as well as nanowires, ribbons, tubes, and rods, either as single structures or in the form of dispersed bundles. For instance, Mitri et al. [51] showed good RT response on PbS-dispersed colloidal QDs towards NO_2 (see Figure 7) with good selectivity, a very low theoretical detection limit of 0.15 ppb, and very good response times, although the recovery is still too long, in the order of several tens of minutes. The overall performance of the device was strongly affected by the thickness of the QD film (Figure 7d), which was controlled by the number of dispersed layers (Figure 7a). This phenomenon was attributed to the fact that sensitivity was expected to increase with thickness layer as more material is able to react to the presence of NO_2 until a certain optimal thickness is reached, from which gas diffusion starts to limit the amount of NO_2 that is capable of reaching the deepest layers. Some works reviewing the room temperature operation of 0D and 1D nanomaterial sensors can be found in Refs [15,16,52,64,78]. Still, most of these devices require high-temperature operation to achieve good sensing performance [33,79].

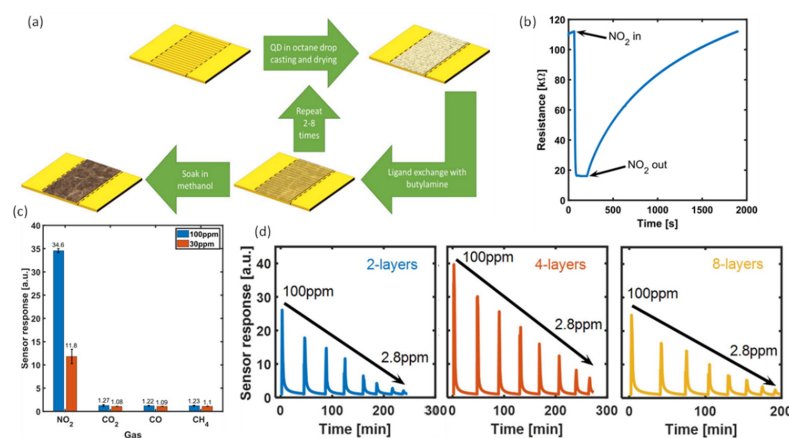


Figure 7. PbS-dispersed colloidal QD sensor for NO_2 detection at RT. (a) Device fabrication process. (b) Signal response to 30 ppm of NO_2 . (c) Selectivity of the device against other pollutants. (d) Effect of film thickness on the performance of the sensor. Adapted with permission from [51]. Copyright by Nature Publishing Group (2020).

With the discovery of graphene and the subsequent explosion of novel 2D materials (2DMs), a new pathway has been opened to achieve RT conductometric gas sensors. 2DMs possess the highest possible surface-to-volume ratio, meaning that any change in their surface properties will affect the entire material. The use of different chemical compositions, other than MOs, opens new opportunities in terms of sensor–analyte interaction and sensing mechanisms. Besides, the peculiar properties of this new class of materials, such as their unique electronic structure or their inherent flexibility and optical transparency, considerably broaden their field of applicability [80]. For instance, graphene sensors were shown to provide an extremely low noise signal, intrinsic of this material, capable of distinguishing single-molecule adsorption events, although with negligible recovery at RT, which required either heating at 150 °C or illuminating the sample with UV light [81]. This is why the number of works and reviews devoted to gas sensors based on 2DMs (hereinafter 2D gas sensors) is increasing at a staggering pace, despite being a relatively recent research field [16,54,80,82–85]. Generally speaking, the transduction, i.e., sensing, mechanism for conductometric 2D gas sensors is simply described as a charge transfer process between the analyte and the 2DM, in contrast to the aforementioned oxygen ionosorption model extensively used to explain the sensing process in MO sensors. Adsorption of analytes is also assumed to be mediated by weak Van der Waals forces, which, in principle, should lead to an easy and fast desorption at RT, facilitating their use as RT sensors with fast response and recovery times [83]. However, this is not always the case, and sometimes, the use of high temperatures or UV light illumination is necessary, even to obtain any recovery at all [81]. In fact, analyte adsorption is strongly affected by the presence of lattice defects, such as vacancies or dopants, as well as some functional groups [41,73,86], which has led to a field of study of its own. For semiconductor 2DMs, such as transition metal dichalcogenides (TMDs), metal dichalcogenides (MD), or graphene oxide (GO), direct charge transfer translates in a shift in their Fermi level, which modifies the concentration of free carriers, the same way as in MOs sensors (Figure 8a,b). For pristine graphene, on the other hand, charge transfer implies a shift in the Fermi level away from Dirac point, which has a minimum in the density of states (DOS), implying an increase in its conductivity [16] (Figure 8c,d). For other metallic 2DMs, such as MXenes, sensing is achieved by the formation of Schottky junctions with a semiconductor (typically a MOs) [84]. In this case, the MXene work function controls the height of the potential barrier and any direct charge transfer from the analyte implies a change in the MXene Fermi level and, therefore, its work function. The use of Schottky junctions as well as van der Waals junctions or 2DM/MOs heterojunctions are also common strategies among 2D gas sensors to enhance the performance of these devices [82–84]. These will be briefly discussed in the following section. Similar to what happens with the oxygen ionosorption model for MO sensors, the general description of weak analyte physisorption and charge transfer in 2DMs is a rough simplification of the overall sensing process. Very often, the sensing mechanisms of 2DMs are not well understood, and sometimes, contradictory results are found throughout the literature. For instance, the role played by lattice defects and/or intentional doping/group functionalization in the sensing mechanisms of 2D sensors has been scarcely investigated [86–88] and more efforts are required in this direction. Besides, the electronic properties of 2DMs as well as their interaction with adsorbates are strongly influenced by their interaction with the substrate [89–92], which may introduce important variations in the sensor performance. Properly understanding the specific sensing mechanisms of these particular materials and the effect of the interaction with the substrate, may be at the core of RT-enhanced gas-sensor operation, not only in single 2DM sensors, but also in more complex heterojunction devices.

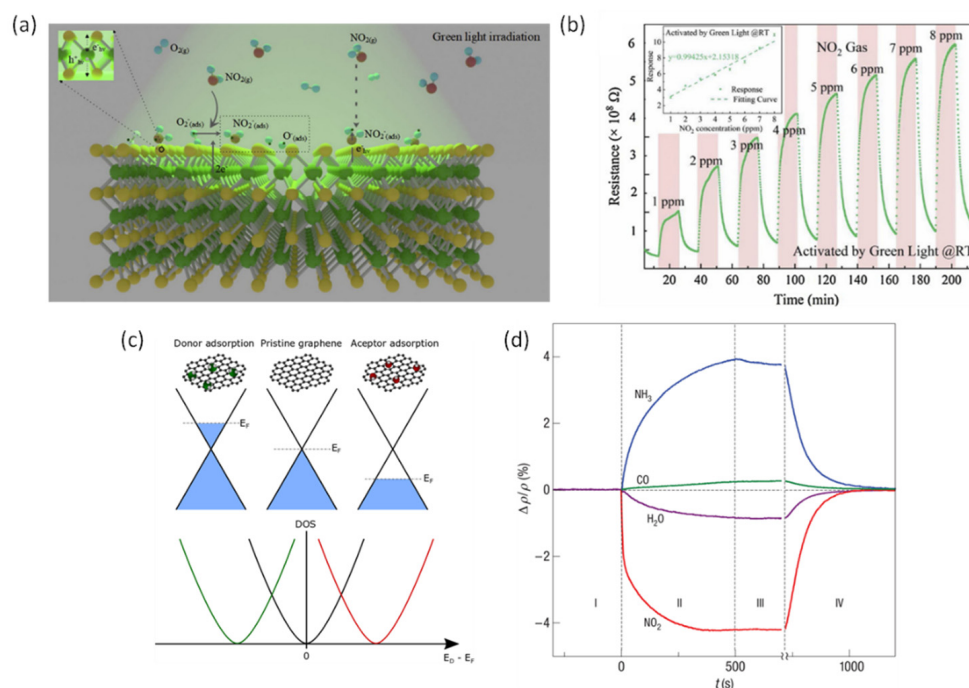


Figure 8. (a,b) Sensing mechanism of SnS₂ 2D nanosheets towards NO₂ and response under green light illumination. Adapted with permission from [53]. Copyright by Elsevier (2020). (c,d) Conductometric sensing mechanism of graphene based on the variation of electronic DOS upon Fermi level variation due to analyte adsorption doping and measured response for different analytes. Adapted with permission from [81]. Copyright by Nature Publishing group (2007).

4.4. Heterojunctions: Schottky, p-n and p-p/n-n Junctions

The use of heterostructures, either by decorating the sensing MOs with metal nanoparticles or by fabricating p-n or n-n/p-p MOs heterojunctions, has also been explored as an alternative to reach room-temperature operation [15,64]. Similarly, the fabrication of 2DM-MOs, 2DM-metal or 2DM-2DM Schottky junctions/heterojunctions is one of the most common strategies to fully exploit the capabilities of 2D materials [54,84,93–95]. The underlying physics behind the sensing performance improvement at room temperature of metal-MO heterostructures are usually different from the remaining heterostructures. In this case, the enhancement is usually achieved via a spillover effect [96], thanks to the higher catalytic activity of the metallic nanoparticles. However, in some cases, the formation of a Schottky barrier at the metal-MO heterojunction has also been exploited to obtain highly non-linear responses that can promote the sensing response at room temperature. This high non-linearity is at the core of p-n or n-n/p-p MOs heterojunction response. The potential barrier formed at the heterojunction drastically determines the conductivity properties of these devices, and the height of the barrier and the width of the space charge region is controlled by each material majority carrier density, which is modulated by their response to the analyte [11,12,26,97–99]. Thus, it is possible to achieve high enough sensitivities to reduce the operation temperature down to RT. Still, the response and recovery times, as well as the interference of humidity in the sensing process, may be an issue. Depending on the band alignment and Fermi level of the components of the heterojunctions, different band bending, and, thus, different sensing characteristics can be achieved (Figure 9).

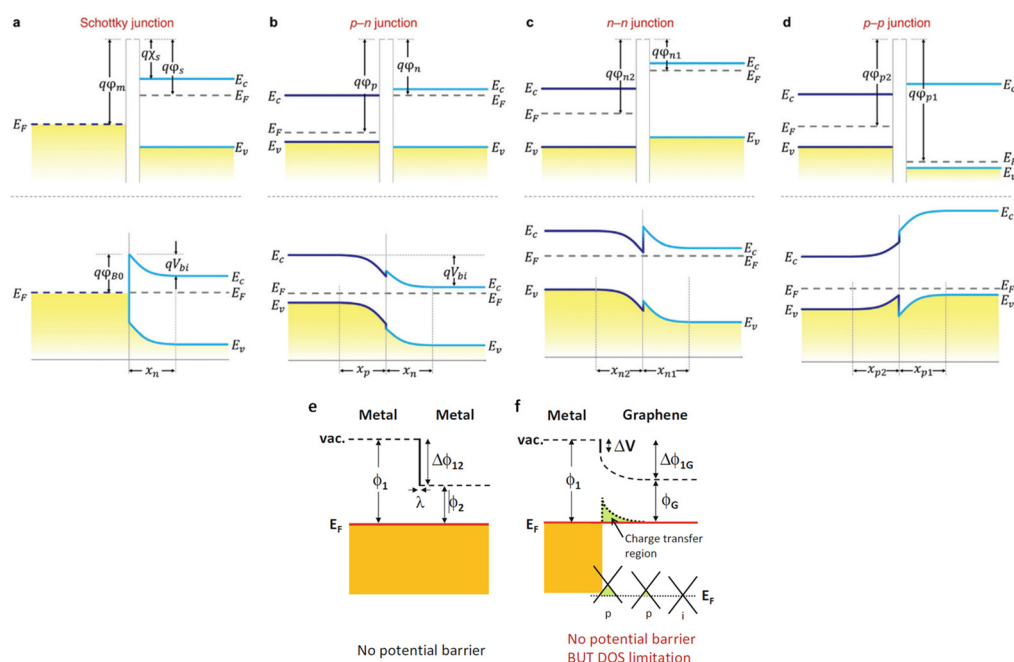


Figure 9. Different band alignment (before junction formation) and band bending (after junction formation) for different types of junctions. (a) Schottky junction. (b) p-n junction. (c) n-n junction. (d) p-p junction. Reproduced with permission from [54]. Copyright by The Royal Society of Chemistry (2019). (e,f) show the difference between metal–metal and metal–graphene contacting, with the latter presenting a charge transfer region responsible for the contact resistance. Adapted with permission from [100]. Copyright by Springer Nature (2015).

Graphene is a particular case as it behaves as a quasi-metallic zero gap material. Thus, direct contacting with other metals should lead to a metal–metal junction. However, owing to its reduced DOS close to the Dirac point, some junction resistance is observed, due to the appearance of a charge transfer region (Figure 9f), the width of which depends on the DOS as $\lambda = [4\pi\text{DOS}(E_F)]^{-1/2}$ [100]. It can also form Schottky contacts with other semiconductors, ranging from conventional MOs (serving either as substrates or as low dimensional structures) [83] to other 2D materials [94].

Control over the Schottky barrier height is essential when dealing with Schottky barrier conductometric sensors. Kim et al. [93] showed that it was possible to properly tune the sensing characteristics of 2D MoS₂ sensors by either changing the electrode material, thus, changing the work function of the electrode, or by changing the number of MoS₂ layers, which determines the bandgap of MoS₂ (Figure 10). They also showed a significant enhancement in the response towards CO and CO₂ by replacing the Au electrode with Ag, going from almost no response at all to 15% sensitivities for 500 and 5000 ppm, respectively.

A different use of a heterojunction barrier formation was demonstrated by Xu et al. [55] on In₂O₃-SnO₂ nanoparticle (NP) composites (Figure 11a) for RT detection of NO_x species. The addition of small portions of In₂O₃ NPs improved the sensitivity of NP SnO₂-based sensors over a factor 11 and, more interestingly, reduced their response times down to a few seconds. Due to their specific band alignment and work function difference, electrons are transferred from In₂O₃ to SnO₂, creating an electron depletion/accumulation region, respectively (Figure 11b,c). The presence of free electrons at the SnO₂ interface enhances the chemisorption and subsequent ionization (i.e., ionosorption) of oxygen species at SnO₂ NP, which, on the one hand, improves its sensitivity towards NO_x species and, on the other hand, facilitates the recovery of the initial state after NO_x has been removed (Figure 11d,e). Thus, in this case, the formation of a heterojunction not only improves the sensitivity of the device but also increases the speed of the sensor response.

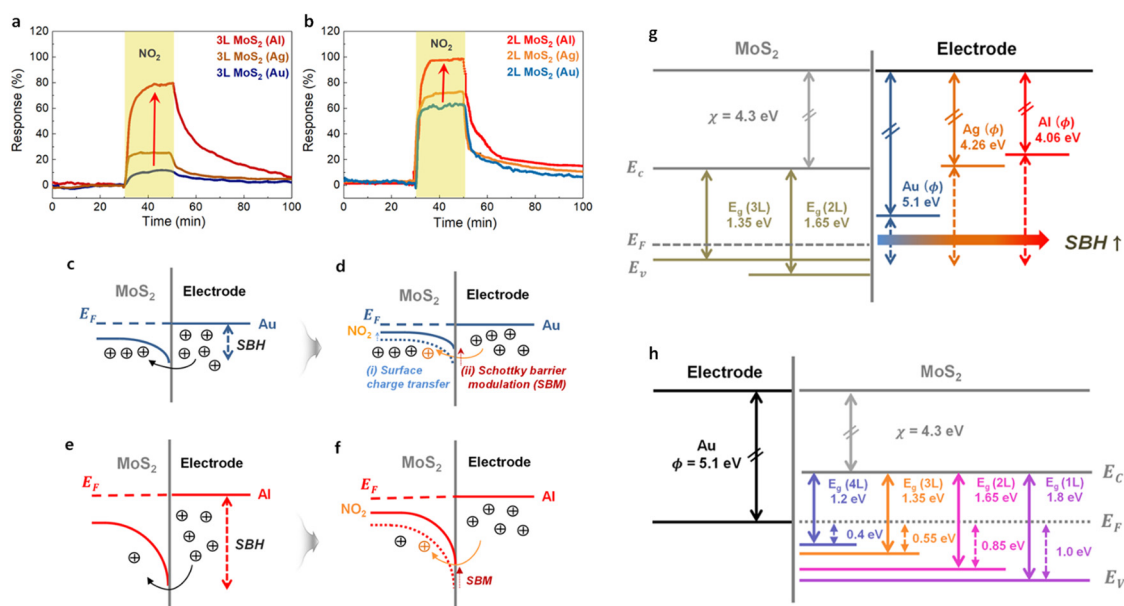


Figure 10. Effect of Schottky barrier height (SBH) engineering on MoS₂-based sensors for NO₂ detection. (a,b) Response towards NO₂ for three different electrodes (metal contact work function) and two different number of MoS₂ layers (semiconductor bandgap). (c–f) Schematic of the Schottky barrier for two different electrodes before and after being exposed to NO₂. (g,h) Band alignment for the different combination of electrodes and number of MoS₂ layers before contacting. Adapted from [93]. Copyright by the American Chemical Society (2019).

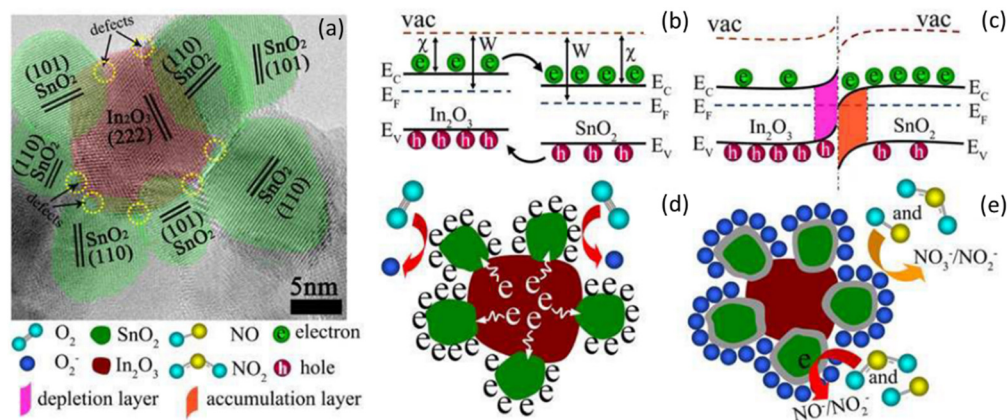


Figure 11. Sensing mechanisms of In₂O₃–SnO₂ nanoparticle (NP) composite heterojunctions. (a) High-resolution transmission electron micrograph of the composite. (b,c) Energy band alignment and bending before and after the junction, respectively. (d,e) Proposed mechanism for the performance enhancement based on the improved oxygen ion sorption caused by the accumulation of free electrons on the SnO₂ NPs from the In₂O₃ NPs. Reproduced with permission from [55]. Copyright by The Royal Society of Chemistry (2015).

4.5. Organic Sensors

An additional approach to design RT conductometric sensors is based on the use of organic materials. In particular, conductive polymers (CP) [59,101–103] and phthalocyanines [15,101] are suitable materials, with great performance, sensitivity and fast time response under low-concentration gas influence, even at room-temperature conditions. Inherent properties of polymers related to their great designability, chemical stability, organic nature, and good mechanical properties allow for a simple approach to fabricate light-weight sensing devices, regarded as low-cost effective due to simple synthe-

sis methods, such as polymerization [16,104,105]. Moreover, due to their affinity with water, they can be diluted in aqueous media, allowing an easy device processing to assemble various morphologies, such as thin layers or nanostructures. Various techniques are employed to assemble polymer-based conductometric sensors, such as dip-coating, spin-coating, doctor blade, thermal evaporation, drop-coating, vapor deposition polymerization, or electrochemical deposition [104]. Among the most promising materials, organic conducting polymers, including polypyrrole (PPy) [102,106], polyaniline (PANI) [107], polythiophene (PTh), poly(phenylene vinylene) (PPV), poly(3,4-ethylenedioxythiophene) (PEDOT), and poly(3,4-ethylenedioxythiophene) polystyrene sulfonate (PEDOT:PSS) and their derivatives [15,59,101,108], are some of the candidates for creating polymeric gas sensing-devices, whose chemical structures are displayed in Figure 12a.

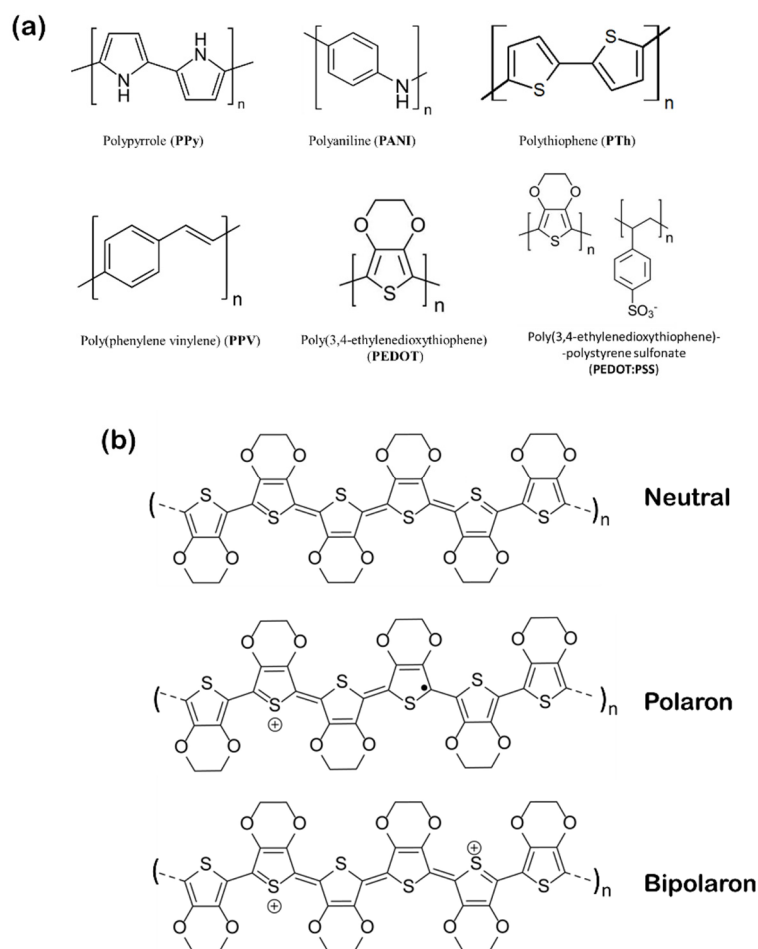


Figure 12. (a) Chemical structures of the most representative conducting polymers used in gas-sensing devices and (b) chemical structure of PEDOT neutral chain, polaron (a radical cation charge carrier), and bipolaron (a di-cation charge carrier).

CPs' gas-sensing working principle is commonly based on the charge transfer between gas molecules and the polymer backbones, which opens the possibility of improving their performance by controlling charge transfer [109]. Their RT performance is mostly related to their electrical conductivity changes due to the affinity with reductive or oxidative gases, which occur even at low temperatures [15]. In fact, unlike MOs, polymer-based sensors could detect many VOCs, such as benzene, which is not chemically reactive with the sensing material at RT, through the measurement of the polymer swelling [110].

Polypyrrole (PPy) was one of the first polymers employed as a gas sensor, most notably for detecting NH_3 gas [59]. The surface of PPy plays a crucial role in the gas-sensing performance as well as its dimensions and morphologies, with thin film [106,111]

nanofibers and nanotubes being the most common [112]. Actually, PPy shows great results as a 1D nanostructure due to the large surface area. This allows one, even for low concentrations (25 ppm) at sufficient RT, to obtain a sensor response of 1.12%, with response times as low as 20 s [106]. PPy also presents great selectivity, being investigated for various analytes, such as H_2 , NO_2 , CO , and $HClV$ [59,111,113].

PEDOT and PEDOT:PSS [103,104,114] are two standpoints on polymeric materials for gas sensing. PEDOT:PSS, which exhibits p-type conductivity, is gaining interest over PEDOT due to its easier processability and higher electrical conductivity. PEDOT:PSS-based sensors have been able to detect different organic analytes, such as NH_3 , CO , CO_2 , NO_2 , as well as ethanol or water vapor [114]. This is particularly interesting for the latter, as PEDOT:PSS films are characterized by a grain-like structure, in which PEDOT grains (conductive) are surrounded by PSS (insulating, hydrophilic), which is linked to the decreasing electrical interconnections among PEDOT chains caused by the water absorption (swelling) of PSS [104]. 1D PEDOT:PSS nanowires can reach high sensitivities of 5.46% and an ultra-fast response of 0.63 s [115].

The sensing mechanism of conducting polymers is directly related to the charge conduction mechanism along the conducting polymer. The conducting polymer structure is composed of conjugated backbones [59], which nominally have a poor conductivity that can be enhanced through appropriate doping [116]. The term doping relates to the concept on inorganic semiconductors, in which the conductivity of a material can be largely increased with the addition of different species in minimum concentrations. These chemical reactants oxidize (or reduce), which modifies the electric conductivity. In a polymer, the overlapping of the π -electron orbitals, composed by delocalized π -electrons alongside the entire chain, contributes to the conductive properties. Doping can enhance the presence of polarons, bipolarons, and solitons (Figure 12b), which create energy states between the HOMO (Highest Occupied Molecular Orbital) and the LUMO (Lowest Unoccupied Molecular Orbital), also affecting the polymer conductivity and, therefore, its sensing properties.

Several sensing mechanisms have been proposed to explain conducting polymer systems, which are often summarized in three groups: (1) redox reaction between the analyte and the chemisorbed oxygen, (2) direct charge transfer between the analyte and the polymer surface and (3) swelling process from the diffusion of the analyte [117], mechanisms which are schematized in Figure 13. These mechanisms can occur either individually or in a combined manner.

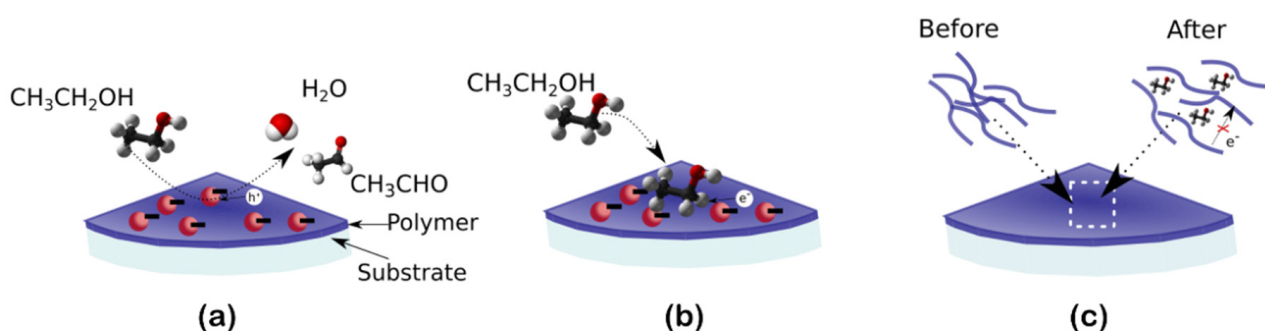


Figure 13. Different gas-sensing mechanism between a reducing analyte (ethanol) and a polymer (e.g., PEDOT:PSS) (a) redox reaction between the analyte and the chemisorbed oxygen on p-type materials, (b) direct charge transfer between the analyte and the polymer surface, and (c) swelling process from the diffusion of the analyte.

The first proposed mechanism consists of the presence of chemisorbed oxygen molecules, which causes electrons to be removed from the conduction band. Those oxygen species are converted into oxygen ions (single or double), which are then ionosorbed. For a p-type material, the hole concentration increases, which causes a decrease in the resistance. When a reducing analyte, such as ethanol or NH_3 (electron-donor), reacts with the ionosorbed

O_2^{ads} , electrons are donated to the conduction band of the p-type material, which reduces the hole concentration and, therefore, the resistance increases. For oxidizing gases, the effect is the contrary and the resistance decreases. For an n-type material, the sensing mechanism becomes the opposite. A classic example is the redox reaction between PPy and ammonia. In the presence of this reducing gas, the p-type PPy suffers a deprotonation, which leads to a decrease in the PPy backbone hole density. As a consequence, the base resistance of the sensor is generally increased [113].



The direct charge transfer process is also responsible for the sensing ability at room temperature of polymers. When, for instance, NH_3 molecules are absorbed by PPy or PEDOT:PSS by physisorption, their hole concentration will interact with the electrons from the analyte and, thus, the overall hole concentration is reduced, following Equations (7) and (8). This leads to the formation of a neutral polymer backbone and a decrease in their major charge carriers will result in a decrease in the electrical conductivity of the film. This mechanism is also responsible for the changes in conductivity on the doping/dedoping processes [59,117], which increase or decrease the charge carrier concentration.

Finally, the swelling process can also affect the sensing performance of such films. In this case, when the analyte molecules diffuse into the polymer matrix, the electron hopping process is blocked as the inter-chain distance increases because of the swelling, reducing the possible conductive pathways.

Doping/dedoping plays a crucial role in the gas-sensing mechanism of the conducting polymer sensors. Doping levels of conducting polymers can be easily changed by chemical reactions at room temperature, which simplifies the detection of analytes. Electron transferring can cause changes in more than just the resistance of the materials, as its work function can be affected, which also plays a significant role on the sensing properties. The most common approaches for doping CP, often referred to as “secondary doping”, implies either (a) the use of organic solvents (film-treatment or blended with the polymer), (b) surfactant addition, or (c) pH modifications (such as acidic treatments) [116], among others. The specific mechanism for enhanced conductivity is the subject of debate. For instance, enhanced conductivity observed in PEDOT:PSS is believed to be due to the partial removal of PSS from PEDOT:PSS and the conformational change in the PEDOT chain from a benzoid coil-like structure to a quinoid linear-like structure, enhancing hopping transport. Other authors attributed the increase in conductivity to the partial replacement of PSS by SO_4^- , which increases the bipolaron population, leading to an increase in the doping level and, thus, the conductivity (Figure 12b) [118]. Recently, the combination of CPs with other nanomaterials to assemble hybrid composites has been a subject of debate [108,110].

4.6. Hybrid Composites: Inorganic/Organic Frameworks

While polymer-based sensing behavior shows great sensitivities at RT, its applicability is hindered due to the relatively low conductivity (which is often lower than 10^{-5} S/cm) [15,101], prior to any doping or treatment, and affinity to different volatile compounds, such as moisture, which can hinder their long-term performance and stability, suffering degradation and unequal performance. Limits on the surface area and non-porous structure of polymers are often pointed out as the reasons for low sensitivity to certain analytes [104]. A possible strategy to overcome these drawbacks is the design of materials based on hybrid inorganic–inorganic [119], organic–organic [120] and, most notably, inorganic–organic materials [114,121], which are connected either by van der Waals or hydrogen bonding interactions or by strong covalent or ionic bonding. These nanocomposites often show novel or enhanced physico-chemical functionalities, attributed to the synergic interaction between the two phases [15,122,123]. In many cases, this allows one to preserve RT-sensing abilities of the organic matrix, while benefiting from the counterpart properties.

The inorganic counterpart can be very diverse [15], from metal oxides [56,109,124–126] metal nanoparticles [83,104,127], carbon nanotubes (CNT) [128], or graphene [16,108], among others. From this combination, a gate is opened to achieve an enhanced mechanism for the precisely designed and optimized sensing performance. These mechanisms for hybrid materials are mainly [121], for inorganics-in-organics, by charge transfer [129], charge carrier transport [64–66] manipulation/construction of heterojunctions [56,109,125,129].

The combination of polymer with metal oxide semiconductors in various forms, such as nanoparticles [108], thin film or fiber [59,126], or core-shell nanoparticles [56], provides an improvement in sensing response based on the synergistic effect among the polymer and the inorganic counterparts. Different metal and metal oxides have been mixed with PPy, PEDOT:PSS, or PANI, such as Au [60], ZnO [103], SnO₂ [124], WO₃ [125], TiO₂ [126], or CeO₂ [56,109]. The observed change in the resistance is due to physical adsorption of the gaseous molecules onto the surface of the nanocomposite film. The interaction of the gas analyte with a π -electron network of a polymer, which has embedded metal or metal oxide nanoparticles, results in the capture/donation of electrons, depending, as mentioned in Section 2, upon the nature of gaseous molecules, either decreasing/increasing resistance [130].

An n-type metal oxide nanoparticle forms a barrier layer with a p-type polymer matrix, creating a depletion region (p-n junction). The schematic of the formed p-n heterojunction is shown in Figure 14a. The improved sensitivity for hybrid composites could be understood by the modulations in the p-n junction [56,131]. In the most common case, conformed by a p-type polymer and an n-type nanoparticle, the space charge region, also known as the depletion layer, is naturally formed by the union of the p-type polymer and the n-type MOs. When exposed to an electron donor, such as ethanol or NH₃, the concentration of holes in the polymer backbone is reduced and the depletion layer increases in size (marked as w_p and w_{p-NH_3} on Figure 14a, respectively), which, in turn, results in a conductivity change [125,132]. This modulation of the space-charge region results in enhanced sensitivity for the desired gas. This working principle is similar for n-n, p-n, p-p, and p-n-p heterojunctions.

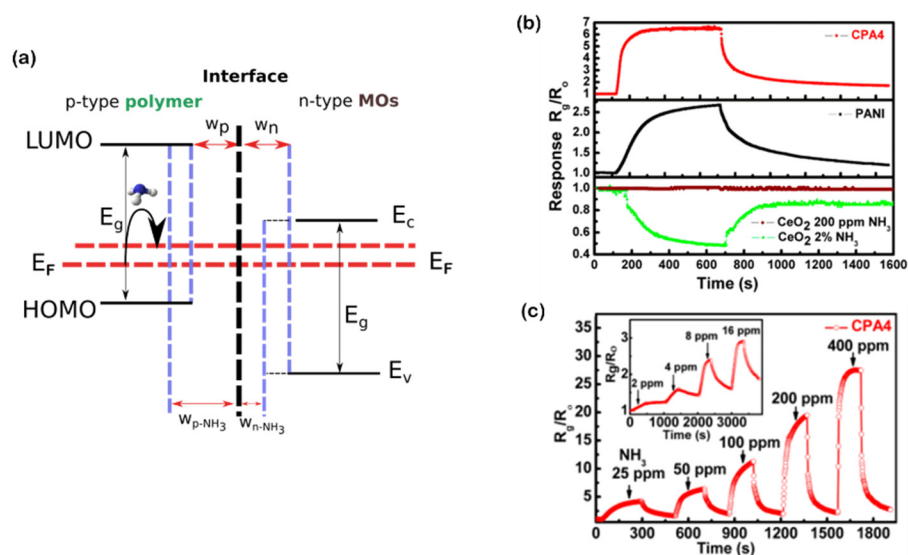


Figure 14. (a) Schematic energy diagram of the p-n junction between a p-type polymer and an n-type MO at equilibrium, when exposed to a reductor gas, such as NH₃. Adapted and modified from [56] and (b) typical response curves of composite containing CeO₂ and PANI (labelled as CPA4), pristine PANI and CeO₂ nanoparticles at RT exposed to 50 ppm of NH₃. (c) The response of the composite at different concentrations. Reproduced with permission from [56]. Copyright by American Chemistry Society (2014).

The creation of heterojunctions between the metal oxide and the polymers, which acts as absorption sites for gas analytes, in combination with a reduction in the signal-to-noise ratio, provides better sensitivity [104]. The sensing mechanism related to charge transfer is different in organic–inorganic frameworks, as charge transfer, in this case, depends not only on intrinsic polymer factors, such as oxidation level or the intra- inter-chain transport, but also on extrinsic factors, which arise because of the nanoparticle–nanoparticle or -metal interaction, playing a significant role [109,114].

In fact, different works have pointed out the importance of the formed heterojunction within the hybrid composite. Wang et al.'s [56] PANI-based sensor using core-shell CeO₂@PANI showed a sensitivity 6.5 to 50 ppm under NH₃ detection and great long-term stability, attributed to the formation of a p-n junction among the nanomaterials through a modification of the space-charge region via the electrons donated by NH₃, which decreased the hole concentration in the PANI, enlarging the depletion layer [56] from w_p to w_{p-NH_3} , as observed in Figure 14. Other effects, such as the conversion of PANI from emeraldine salt (ES) to emeraldine base (EB) due to the NH₃ interaction, can also contribute to the increase in resistance of PANI. As observed in Figure 14b,c, the sensing response of the composite shows a rapid response compared with pristine PANI and the CeO₂ nanoparticles, which is improved with increased NH₃ concentration, the hybrid material being capable of detecting concentrations as low as 2 ppm at RT. Other composites, such as PTh + SnO₂, have shown great sensitivity to NO₂ gas, attributed to the formed p-n junction in addition to the high surface area of the hybrid material [124].

PEDOT:PSS-based composites have also shown an enhancement in the sensitivity against ethanol detection at RT using TiO₂, SnO, or SnO₂ nanoparticles [57,58]. Figure 15 shows a hybrid sensor based on the combination of PEDOT:PSS with ethylene glycol (EG) (as a conductivity enhancer and to enhance nanoparticle dispersion) and with different MO nanoparticles (SnO, SnO, or TiO₂). The performance of the composites under 200 ppm of ethanol gas at RT is shown in the following figures. It must be outlined that SnO nanoparticles exhibit p-type conductivity, while SnO₂ and TiO₂ show n-type conductivity. Figure 15a displays the TEM images of the last two MOs, which average a few nanometers. The polymer was blended with the nanoparticles and deposited by means of spin coating onto a substrate, as shown in Figure 15b,c. Figure 15d shows an example of the resistance changes for the PEDOT:PSS/TiO₂ composite, which is similar for the rest of the composites, as shown in Figure 15f, showing higher sensitivity as compared with the pristine polymer (Figure 15e). However, the highest sensitivity is observed for the composites containing SnO nanoparticles (Figure 15g), attributed to the p-type SnO nature, which could trigger and boost similar sensing mechanisms as for p-type PEDOT:PSS [58].

While we focused this research on polymer/MO composites, not only these materials were considered for hybrid composites. Carbon nanomaterials (CNMs), such as graphene, carbon nanotubes (CNT) or multi-wall carbon nanotubes (MWCNTs) have also been widely employed for chemosensing applications, mainly due to their easily modifiable conductivity, low toxicity, and excellent optoelectronic and mechanical properties, summarized in recent reports [128]. However, by themselves, they present poor results in terms of sensitivity and selectivity and their compounds, with the combination with polymers regarded as some of the most promising materials [128]. In fact, their combination with CPs, such as PEDOT:PSS and polyaniline, allows them to reach sensitivities as high as 28% to NH₃ or NO₂ at 100 ppm [133], as well as a reduction in the recovery time and improved thermal stability [134]. In this case, this phenomenon can be understood due to the physisorption and chemisorption of the analyte molecules by the MWCNT surface. The combination of both inorganic nanoparticles and carbon allotropies has also been considered in recent research. Xiang et al. [135] prepared, by sol–gel and polymerization, a composite containing graphene nanoplatlets (GNs) decorated with TiO₂ nanoparticles (TiO₂@PPy-GN), with a good response to NH₃ gas at RT, attributed to the formation of a p-n junction in the TiO₂ and PPy-GN complex.

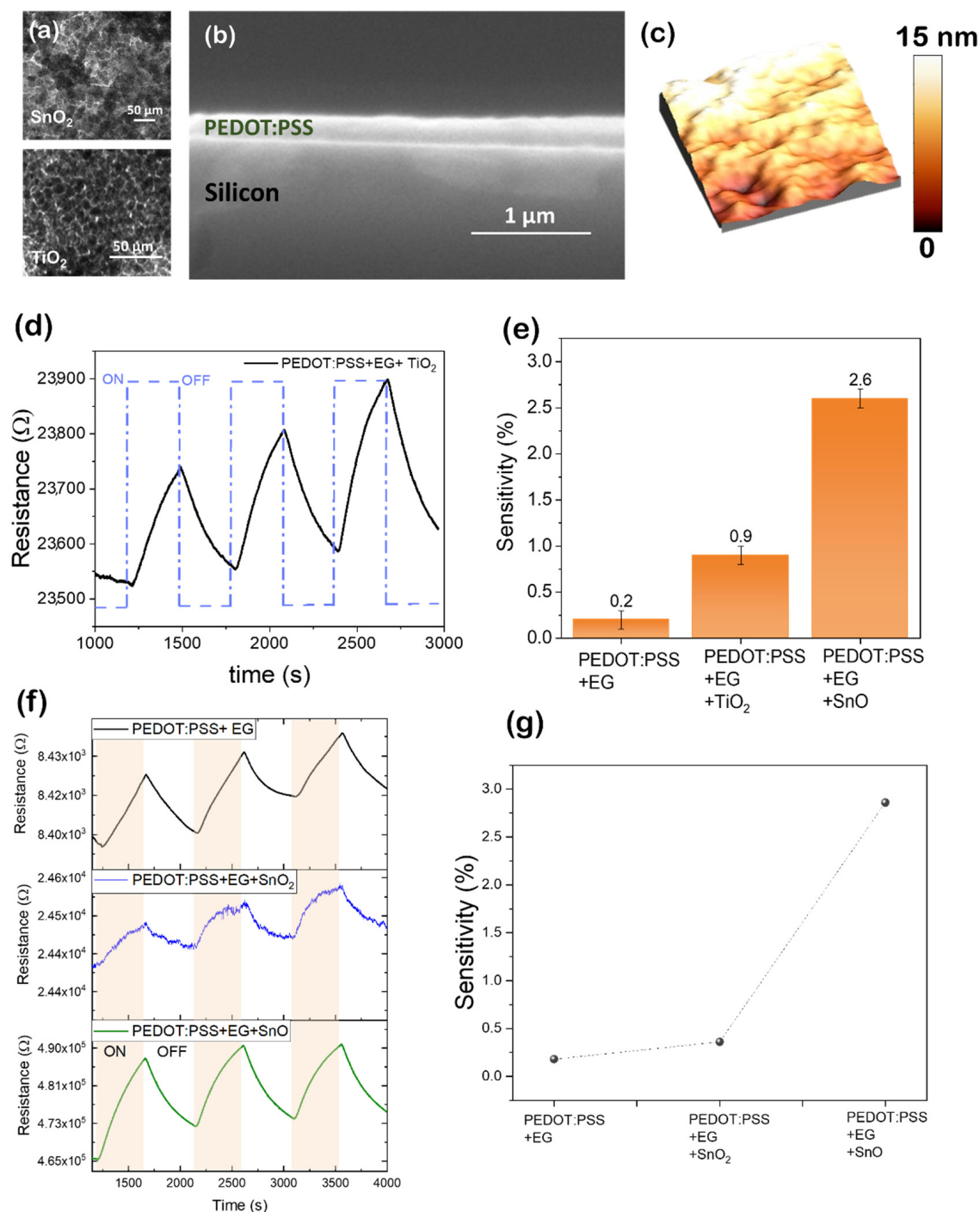


Figure 15. (a) TEM images from SnO₂ and TiO₂ nanoparticles. (b) Cross-sectional SEM image of a PEDOT:PSS layer spin coated onto a Si substrate. (c) AFM image of a PEDOT:PSS layer (d) resistance response at RT of the PEDOT:PSS/TiO₂ composite due to ethanol exposure. (e) Sensitivity of the composites compared with PEDOT:PSS/SnO. Adapted with permission from [57]. Copyright by SPIE (2022). (f) Resistance of the hybrid layers under ethanol exposure and (g) calculated sensitivity for the first cycle of each sample. Adapted with permission from [58]. Copyright by Wiley-VCH (2022).

5. Future Outlook on Conductometric Gas Sensors: Wearable, Self-Heating, and Flexible Sensors

The fast development of technology has pushed gas-sensing technology into various fields. The current technology trends, such as Internet-of-Things (IoT) and 5G, have created

new demand to integrate gas sensors with new devices, such as smartphones, tablets, smart watches, and clothing, to name a few. For those applications, new sensors should fulfill several requirements, such as great flexibility, stability, and low cost, on top of the expected properties of a high-performance device, such as fast response time or sensitivity. In that frame, the achievement of RT operation is considered a favorable condition as well.

The development of flexible gas-sensing devices is gaining increased attention on the market, seeking the possibility of wearable and portable electronic products [80,127]. The main considerations to obtain flexible sensors are selecting the right material and substrate. The material should preserve its sensing abilities despite the strain, stretching, and bending [136]. Currently, substrates can be from plastic, paper, or textile materials [105], while the sensing materials are often polymers, such as polyaniline, polypyrrole, polythiophene (Pth) and poly(3,4-ethylenedioxythiophene) (PEDOT), and PEDOT:PSS, carbon allotropies, such as graphene, transition metal dichalcogenides [80,137], and inorganic/organic hybrid materials [120]. These flexible/wearable sensors have gained substantial interest with the development of technologies, such as e-textiles, in which the sensor can be integrated over/within the textile fabrics [138]. In this field, several works are being conducted regarding the washing, stability, and efficiency of the sensors. For those requirements, inorganic/organic hybrid sensors are among the most promising candidates [120].

Self-heating and energy-saving [138] gas sensors are also a promising trend, which could decrease power consumption [138], especially for MO-based materials. The main idea under self-heating gas sensors is the use of an appropriate voltage, which, via the Joule effect, will generate heat inside the sensor, increasing the temperature and optimizing the sensing working system. Alongside MOs [136], metal-MOs [139] and p-n junctions formed by MOs combined with 2D materials [140] are some of the current candidates. A subset of those self-heating gas sensors can work at RT [139,140].

Finally, machine learning could play a key role in terms of solving some critical issues regarding the sensor operation, such as, for instance, the lack of selectivity from using multiparameter sensors or sensor multi-arrays in combination with deep-learning algorithms for gas discrimination in electronic nose devices [141,142], as well as in future smart sensors. Besides, regulations and safety standards should evolve to undertake the advent of new sensing devices.

6. Conclusions

The advent of a society of ubiquitous sensing in many industries will require gas-sensing systems to be more selective and able to measure lower concentrations of the target gases, including VOC compounds, while involving lower consumption and providing consistent, safe, and reliable performance over longer durations. These challenging tasks, including the development of RT operation sensors, are considered in most of the recent gas-sensing roadmaps. Actually, RT conductometric gas sensors are a trend with expected growth in the near future; however, some challenges must still be faced in order to overcome some of the limitations of these devices in the search for improved stability, selectivity, and sensitivity. This review covers the recent state of the art and progress in the field of gas sensing, with special emphasis on RT operation. In particular, several sensing mechanisms involved in the conductometric sensors' response are reviewed, as well as materials and characterization techniques. Regarding the RT gas sensors, diverse approaches, including light activation, controlled morphology, heterojunctions, as well as the use of organic and hybrid materials, are considered among the common strategies to pursue RT performance. In particular, conductive polymers have shown outstanding results at RT detection, with great selectivity and sensitivity. Furthermore, the combination of inorganics-in-organic led to improved results, mainly related to the formation of p-n junctions and the depletion zone modification during redox processes, which could also be optimized.

Advances in this technology have led to great sensitivity sensors at RT, which now face new desires and challenges due to new technologies. With the improvement in synthesis techniques, assembly, materials selection, and structure design, high-performance and

high-flexibility wearable sensors that can work at RT will be more commonly available in the coming years.

Author Contributions: Investigation, writing, and original draft preparation, A.V.-L. and J.B.; writing, review, and editing, A.V.-L., J.B. and D.M.; conceptualization, A.C. and D.M. All authors have read and agreed to the published version of the manuscript.

Funding: This research was funded by the Spanish Ministry of Innovation and Technology and the Spanish Ministry of Economy through Project RTI2018-097195-B-100. This research received funding from the Comunidad de Madrid and Universidad Autónoma de Madrid under the V PRICIT program through the Project SI3/PJI/2021-00393.

Institutional Review Board Statement: Not applicable.

Informed Consent Statement: Not applicable.

Data Availability Statement: Not applicable.

Acknowledgments: The authors acknowledge collaborators M. Taelño and R. Martínez-Casado for their previous measurements regarding the RT sensing of NiO samples.

Conflicts of Interest: The authors declare no conflict of interest.

References

1. World Health Organization WHO Global Air Quality Guidelines: Particulate Matter (PM_{2.5} and PM₁₀), Ozone, Nitrogen Dioxide, Sulfur Dioxide and Carbon Monoxide; World Health Organization: Geneva, Switzerland, 2021; ISBN 9789240034228.
2. European Environment Agency Air quality standards—European Environment Agency. Available online: <https://www.eea.europa.eu/themes/air/air-quality-concentrations/air-quality-standards> (accessed on 29 November 2021).
3. Ramos, F.; Trilles, S.; Muñoz, A.; Huerta, J. Promoting pollution-free routes in smart cities using air quality sensor networks. *Sensors* **2018**, *18*, 2507. [[CrossRef](#)] [[PubMed](#)]
4. Larkin, A.; Geddes, J.A.; Martin, R.V.; Xiao, Q.; Liu, Y.; Marshall, J.D.; Brauer, M.; Hystad, P. Global Land Use Regression Model for Nitrogen Dioxide Air Pollution. *Environ. Sci. Technol.* **2017**, *51*, 6957–6964. [[CrossRef](#)] [[PubMed](#)]
5. Korotcenkov, G.; Brinzari, V.; Cho, B.K. In₂O₃- and SnO₂-Based Thin Film Ozone Sensors: Fundamentals. *J. Sens.* **2016**, *2016*, 3816094. [[CrossRef](#)]
6. Dey, A. Semiconductor metal oxide gas sensors: A review. *Mater. Sci. Eng. B Solid-State Mater. Adv. Technol.* **2018**, *229*, 206–217. [[CrossRef](#)]
7. Hunter, G.W.; Akbar, S.; Bhansali, S.; Daniele, M.; Erb, P.D.; Johnson, K.; Liu, C.-C.; Miller, D.; Oralkan, O.; Hesketh, P.J.; et al. Editors' Choice—Critical Review—A Critical Review of Solid State Gas Sensors. *J. Electrochem. Soc.* **2020**, *167*, 037570. [[CrossRef](#)]
8. Research, G.V. Global Gas Sensor Market Size & Share Report, 2021–2028. Available online: <https://www.grandviewresearch.com/industry-analysis/gas-sensors-market> (accessed on 29 November 2021).
9. David, M.; Ibrahim, M.H.; Idrus, S.M.; Azmi, A.I.; Ngajikin, N.H.; En Marcus, T.C.; Yaacob, M.; Salim, M.R.; Aziz, A.A. Progress in ozone sensors performance: A review. *J. Teknol.* **2015**, *73*, 23–29. [[CrossRef](#)]
10. Haugen, J.-E.E.; Tomic, O.; Kvaal, K. A calibration method for handling the temporal drift of solid state gas-sensors. *Anal. Chim. Acta* **2000**, *407*, 23–39. [[CrossRef](#)]
11. Hung, C.M.; Le, D.T.T.; Van Hieu, N. On-chip growth of semiconductor metal oxide nanowires for gas sensors: A review. *J. Sci. Adv. Mater. Devices* **2017**, *2*, 263–285. [[CrossRef](#)]
12. Kim, H.J.; Lee, J.H. Highly sensitive and selective gas sensors using p-type oxide semiconductors: Overview. *Sens. Actuators B Chem.* **2014**, *192*, 607–627. [[CrossRef](#)]
13. Moseley, P.T. Progress in the development of semiconducting metal oxide gas sensors: A review. *Meas. Sci. Technol.* **2017**, *28*, 082001. [[CrossRef](#)]
14. Mossaneck, R.J.O.; Domínguez-Cañizares, G.; Gutiérrez, A.; Abbate, M.; Díaz-Fernández, D.; Soriano, L. Effects of Ni vacancies and crystallite size on the O 1s and Ni 2p x-ray absorption spectra of nanocrystalline NiO. *J. Phys. Condens. Matter* **2013**, *25*, 495506. [[CrossRef](#)]
15. Zhang, J.; Liu, X.; Neri, G.; Pinna, N. Nanostructured Materials for Room-Temperature Gas Sensors. *Adv. Mater.* **2016**, *28*, 795–831. [[CrossRef](#)] [[PubMed](#)]
16. Joshi, N.; Hayasaka, T.; Liu, Y.; Liu, H.; Oliveira, O.N.; Lin, L. A review on chemiresistive room temperature gas sensors based on metal oxide nanostructures, graphene and 2D transition metal dichalcogenides. *Microchim. Acta* **2018**, *185*, 213. [[CrossRef](#)] [[PubMed](#)]
17. Zhang, D.; Li, C.; Liu, X.; Man, S.; Tang, T.; Zhou, C. Doping dependent NH₃ sensing of indium oxide nanowires. *Appl. Phys. Lett.* **2003**, *83*, 1845–1847. [[CrossRef](#)]
18. Bartolomé, J.; Taelño, M.; Martínez-Casado, R.; Maestre, D.; Cremades, A. Ethanol gas sensing mechanisms of p-type NiO at room temperature. *Appl. Surf. Sci.* **2022**, *579*, 152134. [[CrossRef](#)]

19. Zhao, C.; Fu, J.; Zhang, Z.; Xie, E. Enhanced ethanol sensing performance of porous ultrathin NiO nanosheets with neck-connected networks. *RSC Adv.* **2013**, *3*, 4018–4023. [[CrossRef](#)]
20. Soumen, D.; Jayaraman, V. SnO₂: A comprehensive review on structures and gas sensors. *Prog. Mater. Sci.* **2014**, *66*, 112–255.
21. Sänze, S.; Hess, C. Ethanol gas sensing by indium oxide: An operando spectroscopic Raman-FTIR study. *J. Phys. Chem. C* **2014**, *118*, 25603–25613. [[CrossRef](#)]
22. Ren, Q.; Cao, Y.-Q.; Arulraj, D.; Liu, C.; Wu, D.; Li, W.-M.; Li, A.-D. Review—Resistive-Type Hydrogen Sensors Based on Zinc Oxide Nanostructures. *J. Electrochem. Soc.* **2020**, *167*, 067528. [[CrossRef](#)]
23. Dai, Z.; Lee, C.S.; Tian, Y.; Kim, I.D.; Lee, J.H. Highly reversible switching from P- to N-type NO₂ sensing in a monolayer Fe₂O₃ inverse opal film and the associated P-N transition phase diagram. *J. Mater. Chem. A* **2015**, *3*, 3372–3381. [[CrossRef](#)]
24. Wang, C.Y.; Cimalla, V.; Kups, T.; Röhlig, C.C.; Romanus, H.; Lebedev, V.; Pezoldt, J.; Stauden, T.; Ambacher, O. Photoreduction and oxidation behavior of In₂O₃ nanoparticles by metal organic chemical vapor deposition. *J. Appl. Phys.* **2007**, *102*, 044310. [[CrossRef](#)]
25. Gurlo, A.; Bârsan, N.; Oprea, A.; Sahm, M.; Sahm, T.; Weimar, U. An n- to p-type conductivity transition induced by oxygen adsorption on α -Fe₂O₃. *Appl. Phys. Lett.* **2004**, *85*, 2280–2282. [[CrossRef](#)]
26. Liang, J.; Lou, Q.; Wu, W.; Wang, K.; Xuan, C. NO₂ Gas Sensing Performance of a VO₂(B) Ultrathin Vertical Nanosheet Array: Experimental and DFT Investigation. *ACS Appl. Mater. Interfaces* **2021**, *13*, 31968–31977. [[CrossRef](#)] [[PubMed](#)]
27. Hübner, M.; Simion, C.E.; Tomescu-Stănoiu, A.; Pokhrel, S.; Bârsan, N.; Weimar, U. Influence of humidity on CO sensing with p-type CuO thick film gas sensors. *Sens. Actuators B Chem.* **2011**, *153*, 347–353. [[CrossRef](#)]
28. Wang, C.Y.; Cimalla, V.; Kups, T.; Röhlig, C.C.; Stauden, T.; Ambacher, O.; Kunzer, M.; Passow, T.; Schirmacher, W.; Pletschen, W.; et al. Integration of In₂O₃ nanoparticle based ozone sensors with GaInN/GaN light emitting diodes. *Appl. Phys. Lett.* **2007**, *91*, 103509. [[CrossRef](#)]
29. Kim, J.H.; Mirzaei, A.; Woo Kim, H.; Kim, S.S. Combination of Pd loading and electron beam irradiation for superior hydrogen sensing of electrospun ZnO nanofibers. *Sens. Actuators B Chem.* **2019**, *284*, 628–637. [[CrossRef](#)]
30. Ganapathi, S.K.; Kaur, M.; Singh, R.; Singh, V.I.; Debnath, A.K.; Muthe, K.P.; Gadkari, S.C. Anomalous Sensing Response of NiO Nanoparticulate Films toward H₂S. *ACS Appl. Nano Mater.* **2019**, *2*, 6726–6737. [[CrossRef](#)]
31. Li, Z.; Wang, N.; Lin, Z.; Wang, J.; Liu, W.; Sun, K.; Fu, Y.Q.; Wang, Z. Room-Temperature High-Performance H₂S Sensor Based on Porous CuO Nanosheets Prepared by Hydrothermal Method. *ACS Appl. Mater. Interfaces* **2016**, *8*, 20962–20968. [[CrossRef](#)]
32. Roso, S.; Degler, D.; Llobet, E.; Bârsan, N.; Urakawa, A. Temperature-Dependent NO₂ Sensing Mechanisms over Indium Oxide. *ACS Sens.* **2017**, *2*, 1272–1277. [[CrossRef](#)]
33. Comini, E. Metal oxide nano-crystals for gas sensing. *Anal. Chim. Acta* **2006**, *568*, 28–40. [[CrossRef](#)]
34. Bârsan, N.; Weimar, U. Conduction model of metal oxide gas sensors. *J. Electroceram.* **2001**, *7*, 143–167. [[CrossRef](#)]
35. Chen, Z.; Lu, C. Humidity sensors: A review of materials and mechanisms. *Sens. Lett.* **2005**, *3*, 274–295. [[CrossRef](#)]
36. Vorokhta, M.; Khalakhan, I.; Vondráček, M.; Tomeček, D.; Vorokhta, M.; Marešová, E.; Nováková, J.; Vlček, J.; Fitl, P.; Novotný, M.; et al. Investigation of gas sensing mechanism of SnO₂ based chemiresistor using near ambient pressure XPS. *Surf. Sci.* **2018**, *677*, 284–290. [[CrossRef](#)]
37. Hozák, P.; Vorokhta, M.; Khalakhan, I.; Jarkovská, K.; Cibulková, J.; Fitl, P.; Vlček, J.; Fara, J.; Tomeček, D.; Novotný, M.; et al. New Insight into the Gas-Sensing Properties of CuOx Nanowires by Near-Ambient Pressure XPS. *J. Phys. Chem. C* **2019**, *123*, 29739–29749. [[CrossRef](#)]
38. Zhao, J.; Li, N.; Yu, H.; Wei, Z.; Liao, M.; Chen, P.; Wang, S.; Shi, D.; Sun, Q.; Zhang, G. Highly Sensitive MoS₂ Humidity Sensors Array for Noncontact Sensation. *Adv. Mater.* **2017**, *29*, 1702076. [[CrossRef](#)]
39. Drozdowska, K.; Welearegay, T.; Österlund, L.; Smulko, J. Combined chemoresistive and in situ FTIR spectroscopy study of nanoporous NiO films for light-activated nitrogen dioxide and acetone gas sensing. *Sens. Actuators B Chem.* **2022**, *353*, 131125. [[CrossRef](#)]
40. Yoo, H.; Heo, K.; Ansari, M.H.R.; Cho, S. Recent Advances in Electrical Doping of 2D Semiconductor Materials: Methods, Analyses, and Applications. *Nanomaterials* **2021**, *11*, 832. [[CrossRef](#)]
41. Cai, B.; Zhang, S.; Yan, Z.; Zeng, H. Noncovalent Molecular Doping of Two-Dimensional Materials. *ChemNanoMat* **2015**, *1*, 542–557. [[CrossRef](#)]
42. Ferrari, A.C.; Basko, D.M. Raman spectroscopy as a versatile tool for studying the properties of graphene. *Nat. Nanotechnol.* **2013**, *8*, 235–246. [[CrossRef](#)]
43. Azcatl, A.; Qin, X.; Prakash, A.; Zhang, C.; Cheng, L.; Wang, Q.; Lu, N.; Kim, M.J.; Kim, J.; Cho, K.; et al. Covalent Nitrogen Doping and Compressive Strain in MoS₂ by Remote N₂ Plasma Exposure. *Nano Lett.* **2016**, *16*, 5437–5443. [[CrossRef](#)]
44. Mignuzzi, S.; Pollard, A.J.; Bonini, N.; Brennan, B.; Gilmore, I.S.; Pimenta, M.A.; Richards, D.; Roy, D. Effect of disorder on Raman scattering of single-layer MoS₂. *Phys. Rev. B* **2015**, *91*, 195411. [[CrossRef](#)]
45. Cheng, G.; Li, B.; Zhao, C.; Yan, X.; Wang, H.; Lau, K.M.; Wang, J. Interfacially Bound Exciton State in a Hybrid Structure of Monolayer WS₂ and InGaN Quantum Dots. *Nano Lett.* **2018**, *18*, 5640–5645. [[CrossRef](#)] [[PubMed](#)]
46. Elger; Hess Application of Raman Spectroscopy to Working Gas Sensors: From in situ to operando Studies. *Sensors* **2019**, *19*, 5075. [[CrossRef](#)] [[PubMed](#)]
47. Yuan, G.; Zhang, H.; Cheng, Y.; Zhong, Y.; Zhuo, Q.; Sun, X. Hollow polyhedral ZnCo₂O₄ superstructure as an ethanol gas sensor and sensing mechanism study using near ambient pressure XPS. *J. Mater. Chem. C* **2021**, *9*, 14278–14285. [[CrossRef](#)]

48. Sabri, Y.M.; Kandjani, A.E.; Rashid, S.S.A.A.H.; Harrison, C.J.; Ippolito, S.J.; Bhargava, S.K. Soot template TiO₂ fractals as a photoactive gas sensor for acetone detection. *Sens. Actuators B Chem.* **2018**, *275*, 215–222. [[CrossRef](#)]
49. de Lacy Costello, B.P.J.; Ewen, R.J.; Ratcliffe, N.M.; Richards, M. Highly sensitive room temperature sensors based on the UV-LED activation of zinc oxide nanoparticles. *Sens. Actuators B Chem.* **2008**, *134*, 945–952. [[CrossRef](#)]
50. Xu, L.; Dong, B.; Wang, Y.; Bai, X.; Liu, Q.; Song, H. Electrospinning preparation and room temperature gas sensing properties of porous In₂O₃ nanotubes and nanowires. *Sens. Actuators B Chem.* **2010**, *147*, 531–538. [[CrossRef](#)]
51. Mitri, F.; De Iacovo, A.; De Luca, M.; Pecora, A.; Colace, L. Lead sulphide colloidal quantum dots for room temperature NO₂ gas sensors. *Sci. Rep.* **2020**, *10*, 12556. [[CrossRef](#)]
52. Ramgir, N.S.; Yang, Y.; Zacharias, M. Nanowire-based sensors. *Small* **2010**, *6*, 1705–1722. [[CrossRef](#)]
53. Gu, D.; Wang, X.; Liu, W.; Li, X.; Lin, S.; Wang, J.; Romyantseva, M.N.; Gaskov, A.M.; Akbar, S.A. Visible-light activated room temperature NO₂ sensing of SnS₂ nanosheets based chemiresistive sensors. *Sens. Actuators B Chem.* **2020**, *305*, 127455. [[CrossRef](#)]
54. Bag, A.; Lee, N.-E. Gas sensing with heterostructures based on two-dimensional nanostructured materials: A review. *J. Mater. Chem. C* **2019**, *7*, 13367–13383. [[CrossRef](#)]
55. Xu, S.; Gao, J.; Wang, L.; Kan, K.; Xie, Y.; Shen, P.; Li, L.; Shi, K. Role of the heterojunctions in In₂O₃-composite SnO₂ nanorod sensors and their remarkable gas-sensing performance for NO_x at room temperature. *Nanoscale* **2015**, *7*, 14643–14651. [[CrossRef](#)] [[PubMed](#)]
56. Wang, L.; Huang, H.; Xiao, S.; Cai, D.; Liu, Y.; Liu, B.; Wang, D.; Wang, C.; Li, H.; Wang, Y.; et al. Enhanced sensitivity and stability of room-temperature NH₃ sensors using core-shell CeO₂ nanoparticles@cross-linked PANI with p-n heterojunctions. *ACS Appl. Mater. Interfaces* **2014**, *6*, 14131–14140. [[CrossRef](#)] [[PubMed](#)]
57. Vázquez-López, A.; García-Alonso, J.; Nahiriak, S.; Bartolomé, J.; Ramírez-Castellanos, J.; Maestre Varea, D.; Saruhan, B.; Cremades, A. Synthesis and characterization of semiconducting oxide nanoparticles and hybrid composites with energy-related applications. In Proceedings of the Oxide-based Materials and Devices XIII, San Francisco, CA, USA, 5 March 2022; Volume 12002, pp. 100–107.
58. Vázquez-López, A.; Bartolomé, J.; Maestre, D.; Cremades, A. Gas Sensing and Thermoelectric Properties of Hybrid Composite Films Based on PEDOT:PSS and SnO or SnO₂ Nanostructures. *Phys. Status Solidi Appl. Mater. Sci.* **2022**, 2100794. [[CrossRef](#)]
59. Wong, Y.C.; Ang, B.C.; Haseeb, A.S.M.A.; Baharuddin, A.A.; Wong, Y.H. Review—Conducting Polymers as Chemiresistive Gas Sensing Materials: A Review. *J. Electrochem. Soc.* **2020**, *167*, 037503. [[CrossRef](#)]
60. Khasim, S.; Pasha, A.; Badi, N.; Ltaief, A.; Al-Ghamdi, S.A.; Panneerselvam, C. Design and development of highly sensitive PEDOT-PSS/AuNP hybrid nanocomposite-based sensor towards room temperature detection of greenhouse methane gas at ppb level. *RSC Adv.* **2021**, *11*, 15017–15029. [[CrossRef](#)]
61. Wang, C.Y.; Becker, R.W.; Passow, T.; Pletschen, W.; Köhler, K.; Cimalla, V.; Ambacher, O. Photon stimulated sensor based on indium oxide nanoparticles I: Wide-concentration-range ozone monitoring in air. *Sens. Actuators B Chem.* **2011**, *152*, 235–240. [[CrossRef](#)]
62. Wang, C.Y.; Bagchi, S.; Bitterling, M.; Becker, R.W.; Köhler, K.; Cimalla, V.; Ambacher, O.; Chaumette, C. Photon stimulated ozone sensor based on indium oxide nanoparticles II: Ozone monitoring in humidity and water environments. *Sens. Actuators B Chem.* **2012**, *164*, 37–42. [[CrossRef](#)]
63. Wang, J.; Shen, H.; Xia, Y.; Komarneni, S. Light-activated room-temperature gas sensors based on metal oxide nanostructures: A review on recent advances. *Ceram. Int.* **2021**, *47*, 7353–7368. [[CrossRef](#)]
64. Cheng, Y.; Ren, B.; Xu, K.; Jeerapan, I.; Chen, H.; Li, Z.; Ou, J.Z. Recent progress in intrinsic and stimulated room-temperature gas sensors enabled by low-dimensional materials. *J. Mater. Chem. C* **2021**, *9*, 3026–3051. [[CrossRef](#)]
65. Kumar, R.; Liu, X.; Zhang, J.; Kumar, M. Room-Temperature Gas Sensors Under Photoactivation: From Metal Oxides to 2D Materials. *Nano-Micro Lett.* **2020**, *12*, 164. [[CrossRef](#)] [[PubMed](#)]
66. Xu, F.; Ho, H.-P. Light-Activated Metal Oxide Gas Sensors: A Review. *Micromachines* **2017**, *8*, 333. [[CrossRef](#)]
67. Sun, X.; Wang, C.; Su, D.; Wang, G.; Zhong, Y. Application of Photocatalytic Materials in Sensors. *Adv. Mater. Technol.* **2020**, *5*, 1900993. [[CrossRef](#)]
68. Melnick, D.A. Zinc oxide photoconduction, an oxygen adsorption process. *J. Chem. Phys.* **1957**, *26*, 1136–1146. [[CrossRef](#)]
69. Peng, L.; Zhao, Q.; Wang, D.; Zhai, J.; Wang, P.; Pang, S.; Xie, T. Ultraviolet-assisted gas sensing: A potential formaldehyde detection approach at room temperature based on zinc oxide nanorods. *Sens. Actuators B Chem.* **2009**, *136*, 80–85. [[CrossRef](#)]
70. Fox, M.A.; Dulay, M.T. Heterogeneous photocatalysis. *Chem. Rev.* **1993**, *93*, 341–357. [[CrossRef](#)]
71. Li, L.; Yang, Y.; Deng, D.; Song, H.; Lv, Y. Photocatalysis enhanced cataluminescence gas sensor for carbon monoxide based on perylenetetracarboxylic diimide. *Sens. Actuators B Chem.* **2020**, *315*, 128080. [[CrossRef](#)]
72. Agrawal, A.V.; Kumar, N.; Kumar, M. Strategy and Future Prospects to Develop Room-Temperature-Recoverable NO₂ Gas Sensor Based on Two-Dimensional Molybdenum Disulfide. *Nano-Micro Lett.* **2021**, *13*, 38. [[CrossRef](#)]
73. Sun, M.; Nelson, A.E.; Adjaye, J. Adsorption and dissociation of H₂ and H₂S on MoS₂ and NiMoS catalysts. *Catal. Today* **2005**, *105*, 36–43. [[CrossRef](#)]
74. Nasriddinov, A.; Tokarev, S.; Fedorova, O.; Bozhev, I.; Romyantseva, M. In₂O₃ Based Hybrid Materials: Interplay between Microstructure, Photoelectrical and Light Activated NO₂ Sensor Properties. *ChemoSens.* **2022**, *10*, 135. [[CrossRef](#)]

75. Chizhov, A.S.; Romyantseva, M.N.; Vasiliev, R.B.; Filatova, D.G.; Drozdov, K.A.; Krylov, I.V.; Marchevsky, A.V.; Karakulina, O.M.; Abakumov, A.M.; Gaskov, A.M. Visible light activation of room temperature NO₂ gas sensors based on ZnO, SnO₂ and In₂O₃ sensitized with CdSe quantum dots. *Thin Solid Films* **2016**, *618*, 253–262. [[CrossRef](#)]
76. Qomaruddin; Casals, O.; Wasisto, H.S.; Waag, A.; Prades, J.D.; Fàbrega, C. Visible-Light-Driven Room Temperature NO₂ Gas Sensor Based on Localized Surface Plasmon Resonance: The Case of Gold Nanoparticle Decorated Zinc Oxide Nanorods (ZnO NRs). *ChemoSens* **2022**, *10*, 28. [[CrossRef](#)]
77. Bhaduri, A.; Singh, S.; Thapa, K.B.; Yadav, B.C. Visible light-induced, highly responsive, below lower explosive limit (LEL) LPG sensor based on hydrothermally synthesized barium hexaferrite nanorods. *Sens. Actuators B Chem.* **2021**, *348*, 130714. [[CrossRef](#)]
78. Galstyan, V. “Quantum dots: Perspectives in next-generation chemical gas sensors”—A review. *Anal. Chim. Acta* **2021**, *1152*, 238192. [[CrossRef](#)]
79. Huang, X.J.; Choi, Y.K. Chemical sensors based on nanostructured materials. *Sens. Actuators B Chem.* **2007**, *122*, 659–671. [[CrossRef](#)]
80. Kumar, R.; Goel, N.; Hojamberdiev, M.; Kumar, M. Transition metal dichalcogenides-based flexible gas sensors. *Sens. Actuators A Phys.* **2020**, *303*, 111875. [[CrossRef](#)]
81. Schedin, F.; Geim, A.K.; Morozov, S.V.; Hill, E.W.; Blake, P.; Katsnelson, M.I.; Novoselov, K.S. Detection of individual gas molecules adsorbed on graphene. *Nat. Mater.* **2007**, *6*, 652–655. [[CrossRef](#)]
82. Zheng, W.; Liu, X.; Xie, J.; Lu, G.; Zhang, J. Emerging van der Waals junctions based on TMDs materials for advanced gas sensors. *Coord. Chem. Rev.* **2021**, *447*, 214151. [[CrossRef](#)]
83. Bhati, V.S.; Kumar, M.; Banerjee, R. Gas sensing performance of 2D nanomaterials/metal oxide nanocomposites: A review. *J. Mater. Chem. C* **2021**, *9*, 8776–8808. [[CrossRef](#)]
84. Mathew, M.; Rout, C.S. Schottky diodes based on 2D materials for environmental gas monitoring: A review on emerging trends, recent developments and future perspectives. *J. Mater. Chem. C* **2021**, *9*, 395–416. [[CrossRef](#)]
85. Zhang, J.; Liu, L.; Yang, Y.; Huang, Q.; Li, D.; Zeng, D. A review on two-dimensional materials for chemiresistive- and FET-type gas sensors. *Phys. Chem. Chem. Phys.* **2021**, *23*, 15420–15439. [[CrossRef](#)] [[PubMed](#)]
86. You, Y.; Deng, J.; Tan, X.; Gorjizadeh, N.; Yoshimura, M.; Smith, S.C.; Sahajwalla, V.; Joshi, R.K. On the mechanism of gas adsorption for pristine, defective and functionalized graphene. *Phys. Chem. Chem. Phys.* **2017**, *19*, 6051–6056. [[CrossRef](#)] [[PubMed](#)]
87. Park, S.Y.; Kim, Y.H.; Lee, S.Y.; Sohn, W.; Lee, J.E.; Kim, D.H.; Shim, Y.-S.; Kwon, K.C.; Choi, K.S.; Yoo, H.J.; et al. Highly selective and sensitive chemoresistive humidity sensors based on rGO/MoS₂ van der Waals composites. *J. Mater. Chem. A* **2018**, *6*, 5016–5024. [[CrossRef](#)]
88. Kaewmaraya, T.; Ngamwongwan, L.; Moontragoon, P.; Karton, A.; Hussain, T. Drastic Improvement in Gas-Sensing Characteristics of Phosphorene Nanosheets under Vacancy Defects and Elemental Functionalization. *J. Phys. Chem. C* **2018**, *122*, 20186–20193. [[CrossRef](#)]
89. Bartolomé, J.; Álvarez-Fraga, L.; Aguilar-Pujol, M.X.; Cortijo, S.; Cremades, A.; Prieto, C.; De Andrés, A. Grain selective Cu oxidation and anomalous shift of graphene 2D Raman peak in the graphene-Cu system. *2D Mater.* **2019**, *6*, 015023. [[CrossRef](#)]
90. Choi, J.; Koo, S.; Song, M.; Jung, D.Y.; Choi, S.Y.; Ryu, S. Varying electronic coupling at graphene-copper interfaces probed with Raman spectroscopy. *2D Mater.* **2020**, *7*, 025006. [[CrossRef](#)]
91. Kumar, B.; Min, K.; Bashirzadeh, M.; Farimani, A.B.; Bae, M.-H.; Estrada, D.; Kim, Y.D.; Yasaei, P.; Park, Y.D.; Pop, E.; et al. The Role of External Defects in Chemical Sensing of Graphene Field-Effect Transistors. *Nano Lett.* **2013**, *13*, 1962–1968. [[CrossRef](#)]
92. Sun, T.-Y.; Hao, Y.; Lin, C.-T.; Wang, L.; Huang, L.-F. Unraveling the strong coupling between graphene/nickel interface and atmospheric adsorbates for versatile realistic applications. *Carbon Trends* **2021**, *2*, 100013. [[CrossRef](#)]
93. Kim, Y.; Kang, S.-K.; Oh, N.-C.; Lee, H.-D.; Lee, S.-M.; Park, J.; Kim, H. Improved Sensitivity in Schottky Contacted Two-Dimensional MoS₂ Gas Sensor. *ACS Appl. Mater. Interfaces* **2019**, *11*, 38902–38909. [[CrossRef](#)]
94. Yuan, S.; Zhang, S. Recent progress on gas sensors based on graphene-like 2D/2D nanocomposites. *J. Semicond.* **2019**, *40*, 111608. [[CrossRef](#)]
95. Latif, U.; Dickert, F.L. Graphene hybrid materials in gas sensing applications. *Sensors* **2015**, *15*, 30504–30524. [[CrossRef](#)] [[PubMed](#)]
96. Xing, R.; Xu, L.; Song, J.; Zhou, C.; Li, Q.; Liu, D.; Song, H.W. Preparation and gas sensing properties of In₂O₃/Au nanorods for detection of volatile organic compounds in exhaled breath. *Sci. Rep.* **2015**, *5*, 10717. [[CrossRef](#)] [[PubMed](#)]
97. Chen, Y.; Shen, Z.; Jia, Q.; Zhao, J.; Zhao, Z.; Ji, H. A CuO-ZnO nanostructured p-n junction sensor for enhanced N-butanol detection. *RSC Adv.* **2016**, *6*, 2504–2511. [[CrossRef](#)]
98. Tang, H.; Li, Y.; Sokolovskij, R.; Sacco, L.; Zheng, H.; Ye, H.; Yu, H.; Fan, X.; Tian, H.; Ren, T.-L.; et al. Ultra-High Sensitive NO₂ Gas Sensor Based on Tunable Polarity Transport in CVD-WS₂/IGZO p-N Heterojunction. *ACS Appl. Mater. Interfaces* **2019**, *11*, 40850–40859. [[CrossRef](#)]
99. Han, Y.; Liu, Y.; Su, C.; Wang, S.; Li, H.; Zeng, M.; Hu, N.; Su, Y.; Zhou, Z.; Wei, H.; et al. Interface engineered WS₂/ZnS heterostructures for sensitive and reversible NO₂ room temperature sensing. *Sens. Actuators B Chem.* **2019**, *296*, 126666. [[CrossRef](#)]
100. Matsumoto, K. *Frontiers of Graphene and Carbon Nanotubes: Devices and Applications*; Springer: Berlin/Heidelberg, Germany, 2015; pp. 1–289.
101. Bai, H.; Shi, G. Gas Sensors Based on Conducting Polymers. *Sensors* **2007**, *7*, 267–307. [[CrossRef](#)]
102. Ramanavičius, A.; Ramanavičiene, A.; Malinauskas, A. Electrochemical sensors based on conducting polymer—Polypyrrole. *Electrochim. Acta* **2006**, *51*, 6025–6037. [[CrossRef](#)]

103. Wang, Y.; Liu, A.; Han, Y.; Li, T. Sensors based on conductive polymers and their composites: A review. *Polym. Int.* **2020**, *69*, 7–17. [[CrossRef](#)]
104. Gao, N.; Yu, J.; Tian, Q.; Shi, J.; Zhang, M.; Chen, S.; Zang, L. Application of PEDOT:PSS and Its Composites in Electrochemical and Electronic Chemosensors. *ChemoSens.* **2021**, *9*, 79. [[CrossRef](#)]
105. Alrammouz, R.; Podlecki, J.; Abboud, P.; Sorli, B.; Habchi, R. A review on flexible gas sensors: From materials to devices. *Sens. Actuators A Phys.* **2018**, *284*, 209–231. [[CrossRef](#)]
106. Joshi, A.; Gangal, S.A.; Gupta, S.K. Ammonia sensing properties of polypyrrole thin films at room temperature. *Sens. Actuators B Chem.* **2011**, *156*, 938–942. [[CrossRef](#)]
107. Wan, N.; Lu, X.; Wang, Y.; Zhang, W.; Bai, Y.; Hu, Y.S.; Dai, S. Improved Li storage performance in SnO₂ nanocrystals by a synergetic doping. *Sci. Rep.* **2016**, *6*, 18978. [[CrossRef](#)] [[PubMed](#)]
108. Yan, Y.; Yang, G.; Xu, J.L.; Zhang, M.; Kuo, C.C.; Wang, S.D. Conducting polymer-inorganic nanocomposite-based gas sensors: A review. *Sci. Technol. Adv. Mater.* **2020**, *21*, 768–786. [[CrossRef](#)] [[PubMed](#)]
109. Park, S.J.; Park, C.S.; Yoon, H. Chemo-Electrical Gas Sensors Based on Conducting Polymer Hybrids. *Polymers* **2017**, *9*, 155. [[CrossRef](#)]
110. Nazemi, H.; Joseph, A.; Park, J.; Emadi, A. Advanced Micro- and Nano-Gas Sensor Technology: A Review. *Sensors* **2019**, *19*, 1285. [[CrossRef](#)]
111. Navale, S.T.; Mane, A.T.; Chougule, M.A.; Sakhare, R.D.; Nalage, S.R.; Patil, V.B. Highly selective and sensitive room temperature NO₂ gas sensor based on polypyrrole thin films. *Synth. Met.* **2014**, *189*, 94–99. [[CrossRef](#)]
112. Yoon, H.; Chang, M.; Jang, J. Sensing Behaviors of Polypyrrole Nanotubes Prepared in Reverse Microemulsions: Effects of Transducer Size and Transduction Mechanism. *J. Phys. Chem. B* **2006**, *110*, 14074–14077. [[CrossRef](#)]
113. Das, M.; Roy, S. Polypyrrole and associated hybrid nanocomposites as chemiresistive gas sensors: A comprehensive review. *Mater. Sci. Semicond. Process.* **2021**, *121*, 105332. [[CrossRef](#)]
114. Yoon, H.; Hong, J.Y.; Jang, J. Charge-Transport Behavior in Shape-Controlled Poly(3,4-ethylenedioxythiophene) Nanomaterials: Intrinsic and Extrinsic Factors. *Small* **2007**, *3*, 1774–1783. [[CrossRef](#)]
115. Zhou, C.; Zhang, X.; Tang, N.; Fang, Y.; Zhang, H.; Duan, X. Rapid response flexible humidity sensor for respiration monitoring using nano-confined strategy. *Nanotechnology* **2020**, *31*, 125302. [[CrossRef](#)]
116. Shi, H.; Liu, C.; Jiang, Q.; Xu, J. Effective Approaches to Improve the Electrical Conductivity of PEDOT:PSS: A Review. *Adv. Electron. Mater.* **2015**, *1*, 1500017. [[CrossRef](#)]
117. Seekaew, Y.; Lokavee, S.; Phokharatkul, D.; Wisitorsaat, A.; Kerdcharoen, T.; Wongchoosuk, C. Low-cost and flexible printed graphene-PEDOT:PSS gas sensor for ammonia detection. *Org. Electron.* **2014**, *15*, 2971–2981. [[CrossRef](#)]
118. Reyes-Reyes, M.; Cruz-Cruz, I.; López-Sandoval, R. Enhancement of the electrical conductivity in PEDOT: PSS films by the addition of dimethyl sulfate. *J. Phys. Chem. C* **2010**, *114*, 20220–20224. [[CrossRef](#)]
119. Korotcenkov, G.; Cho, B.K. Metal oxide composites in conductometric gas sensors: Achievements and challenges. *Sens. Actuators B Chem.* **2017**, *244*, 182–210. [[CrossRef](#)]
120. Ren, Z.; Yang, J.; Qi, D.; Sonar, P.; Liu, L.; Lou, Z.; Shen, G.; Wei, Z.; Ren, Z.; Yang, J.; et al. Flexible Sensors Based on Organic–Inorganic Hybrid Materials. *Adv. Mater. Technol.* **2021**, *6*, 2000889. [[CrossRef](#)]
121. Ma, L.J.; Li, Y.X.; Yu, X.F.; Yang, Q.B.; Noh, C.H. Using room temperature ionic liquid to fabricate PEDOT/TiO₂ nanocomposite electrode-based electrochromic devices with enhanced long-term stability. *Sol. Energy Mater. Sol. Cells* **2008**, *92*, 1253–1259. [[CrossRef](#)]
122. Vázquez-López, A.; Yaseen, A.; Maestre, D.; Ramírez-Castellanos, J.; Marstein, E.S.; Karazhanov, S.Z.; Cremades, A. Synergetic Improvement of Stability and Conductivity of Hybrid Composites formed by PEDOT:PSS and SnO Nanoparticles. *Molecules* **2020**, *25*, 695. [[CrossRef](#)]
123. Vázquez-López, A.; Yaseen, A.; Maestre, D.; Ramírez-Castellanos, J.; Karazhanov, S.Z.; Marstein, E.S.; Cremades, A. Improved silicon surface passivation by hybrid composites formed by PEDOT:PSS with anatase TiO₂ nanoparticles. *Mater. Lett.* **2020**, *271*, 127802. [[CrossRef](#)]
124. Xu, M.; Zhang, J.; Wang, S.; Guo, X.; Xia, H.; Wang, Y.; Zhang, S.; Huang, W.; Wu, S. Gas sensing properties of SnO₂ hollow spheres/polythiophene inorganic–organic hybrids. *Sens. Actuators B Chem.* **2010**, *146*, 8–13. [[CrossRef](#)]
125. Kaushik, A.; Khan, R.; Gupta, V.; Malhotra, B.D.; Ahmad, S.; Singh, S.P. Hybrid Cross-Linked Polyaniline-WO₃ Nanocomposite Thin Film for NO_x Gas Sensing. *J. Nanosci. Nanotechnol.* **2009**, *9*, 1792–1796. [[CrossRef](#)]
126. Zampetti, E.; Pantalei, S.; Muzyczuk, A.; Bearzotti, A.; De Cesare, F.; Spinella, C.; Macagnano, A. A high sensitive NO₂ gas sensor based on PEDOT-PSS/TiO₂ nanofibres. *Sens. Actuators B Chem.* **2013**, *176*, 390–398. [[CrossRef](#)]
127. Bag, A.; Lee, N.E. Recent Advancements in Development of Wearable Gas Sensors. *Adv. Mater. Technol.* **2021**, *6*, 1–37. [[CrossRef](#)]
128. Dariyal, P.; Sharma, S.; Chauhan, G.S.; Singh, B.P.; Dhakate, S.R. Recent trends in gas sensing via carbon nanomaterials: Outlook and challenges. *Nanoscale Adv.* **2021**, *3*, 6514–6544. [[CrossRef](#)]
129. Guo, Y.; Wang, T.; Chen, F.; Sun, X.; Li, X.; Yu, Z.; Wan, P.; Chen, X. Hierarchical graphene–polyaniline nanocomposite films for high-performance flexible electronic gas sensors. *Nanoscale* **2016**, *8*, 12073–12080. [[CrossRef](#)]
130. Kaushik, A.; Kumar, R.; Arya, S.K.; Nair, M.; Malhotra, B.D.; Bhansali, S. Organic–Inorganic Hybrid Nanocomposite-Based Gas Sensors for Environmental Monitoring. *Chem. Rev.* **2015**, *115*, 4571–4606. [[CrossRef](#)]

131. Ho, T.A.; Jun, T.S.; Kim, Y.S. Material and NH₃-sensing properties of polypyrrole-coated tungsten oxide nanofibers. *Sens. Actuators B Chem.* **2013**, *185*, 523–529. [[CrossRef](#)]
132. Ram, M.K.; Yavuz, O.; Aldissi, M. NO₂ gas sensing based on ordered ultrathin films of conducting polymer and its nanocomposite. *Synth. Met.* **2005**, *151*, 77–84. [[CrossRef](#)]
133. Mangu, R.; Rajaputra, S.; Singh, V.P. MWCNT–polymer composites as highly sensitive and selective room temperature gassensors. *Nanotechnology* **2011**, *22*, 215502. [[CrossRef](#)]
134. Sharma, S.; Hussain, S.; Singh, S.; Islam, S.S. MWCNT-conducting polymer composite based ammonia gas sensors: A new approach for complete recovery process. *Sens. Actuators B Chem.* **2014**, *194*, 213–219. [[CrossRef](#)]
135. Xiang, C.; Jiang, D.; Zou, Y.; Chu, H.; Qiu, S.; Zhang, H.; Xu, F.; Sun, L.; Zheng, L. Ammonia sensor based on polypyrrole–graphene nanocomposite decorated with titania nanoparticles. *Ceram. Int.* **2015**, *41*, 6432–6438. [[CrossRef](#)]
136. Ngoc, T.M.; Van Duy, N.; Duc Hoa, N.; Manh Hung, C.; Nguyen, H.; Van Hieu, N. Effective design and fabrication of low-power-consumption self-heated SnO₂ nanowire sensors for reducing gases. *Sens. Actuators B Chem.* **2019**, *295*, 144–152. [[CrossRef](#)]
137. Goswami, P.; Gupta, G. Recent progress of flexible NO₂ and NH₃ gas sensors based on transition metal dichalcogenides for room temperature sensing. *Mater. Today Chem.* **2022**, *23*, 100726. [[CrossRef](#)]
138. Majhi, S.M.; Mirzaei, A.; Kim, H.W.; Kim, S.S.; Kim, T.W. Recent advances in energy-saving chemiresistive gas sensors: A review. *Nano Energy* **2021**, *79*, 105369. [[CrossRef](#)]
139. Arunkumar, S.; Hou, T.; Kim, Y.B.; Choi, B.; Park, S.H.; Jung, S.; Lee, D.W. Au Decorated ZnO hierarchical architectures: Facile synthesis, tunable morphology and enhanced CO detection at room temperature. *Sens. Actuators B Chem.* **2017**, *243*, 990–1001. [[CrossRef](#)]
140. Jayababu, N.; Poloju, M.; Shruthi, J.; Reddy, M.V.R. Semi shield driven p-n heterostructures and their role in enhancing the room temperature ethanol gas sensing performance of NiO/SnO₂ nanocomposites. *Ceram. Int.* **2019**, *45*, 15134–15142. [[CrossRef](#)]
141. Hayasaka, T.; Lin, A.; Copa, V.C.; Lopez, L.P.; Loberternos, R.A.; Ballesteros, L.I.M.; Kubota, Y.; Liu, Y.; Salvador, A.A.; Lin, L. An electronic nose using a single graphene FET and machine learning for water, methanol, and ethanol. *Microsyst. Nanoeng.* **2020**, *6*, 50. [[CrossRef](#)]
142. Kang, M.; Cho, I.; Park, J.; Jeong, J.; Lee, K.; Lee, B.; Del Orbe Henriquez, D.; Yoon, K.; Park, I. High Accuracy Real-Time Multi-Gas Identification by a Batch-Uniform Gas Sensor Array and Deep Learning Algorithm. *ACS Sens.* **2022**, *7*, 430–440. [[CrossRef](#)]